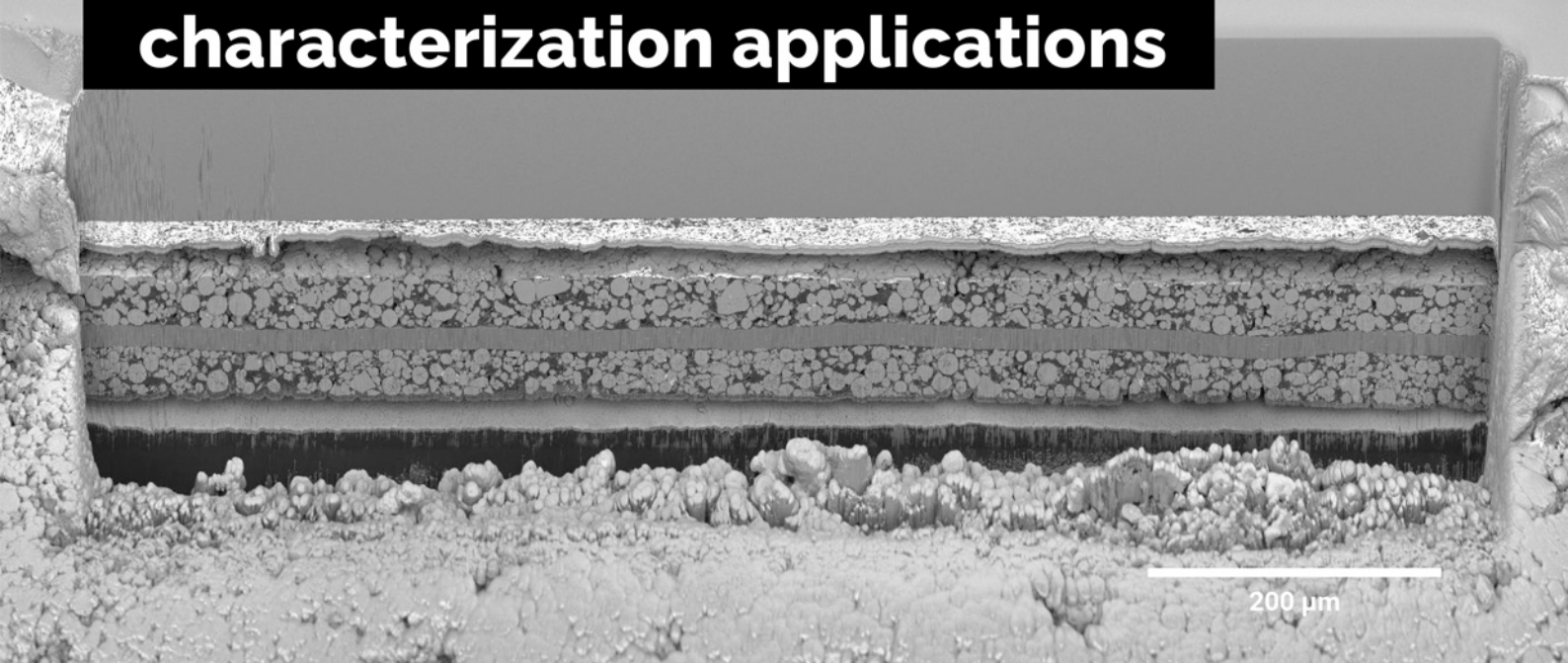


A unique combination of Plasma FIB and field-free UHR SEM for the widest range of multiscale materials characterization applications



1 mm cross-section through a Li-ion battery electrode

TESCAN AMBER X

- ✓ High throughput, large area FIB milling up to 1 mm
- ✓ Ga-free microsample preparation
- ✓ Ultra-high resolution, field-free FE-SEM imaging and analysis
- ✓ In-column SE and BSE detection
- ✓ Spot optimization for high-throughput, multi-modal FIB-SEM tomography
- ✓ Superior field of view for easy navigation
- ✓ Essence™ easy-to-use, modular graphical user interface



For more information visit

www.tescan.com

Designing Cathodes and Cathode Active Materials for Solid-State Batteries

Philip Minnmann, Florian Strauss, Anja Bielefeld, Raffael Ruess, Philipp Adelhelm, Simon Burkhardt, Sören L. Dreyer, Enrico Trevisanello, Helmut Ehrenberg, Torsten Brezesinski,* Felix H. Richter,* and Jürgen Janek*

Solid-state batteries (SSBs) currently attract great attention as a potentially safe electrochemical high-energy storage concept. However, several issues still prevent SSBs from outperforming today's lithium-ion batteries based on liquid electrolytes. One major challenge is related to the design of cathode active materials (CAMs) that are compatible with the superionic solid electrolytes (SEs) of interest. This perspective, gives a brief overview of the required properties and possible challenges for inorganic CAMs employed in SSBs, and describes state-of-the-art solutions. In particular, the issue of tailoring CAMs is structured into challenges arising on the cathode-, particle-, and interface-level, related to microstructural, (chemo-)mechanical, and (electro-)chemical interplay of CAMs with SEs, and finally guidelines for future CAM development for SSBs are proposed.

material (CAM) in its lithiated form, that is, as present in a discharged cell. In its delithiated form, when the cell is charged, it is the only cell component that is contributing to storing energy (in conjunction with a hypothetical in situ lithium-plated anode formed during charging), thus making it the material required to be present in large quantity to achieve a high-performing cell. All other components, which may be required for large scale processing, only decrease the specific energy of the cell and are, therefore, engineered to minimize their content without affecting the function of the cell. This is evident in the research efforts made

1. Introduction

The increasing demand for safe, reliable, and affordable energy-storage devices has stimulated extensive battery research and development in the last decade. While the development of conventional lithium-ion batteries (LIBs) using organic liquid electrolytes (LEs) is approaching physicochemical limits, solid-state batteries (SSBs) with high capacity anodes (e.g., Li metal) are considered as a promising alternative, and their commercialization within the near future is strongly anticipated.^[1–3]


The key component of any battery, regardless of whether utilizing LEs or solid electrolytes (SEs), is the cathode active

to increase the CAM content in the cathode layer, decrease the separator thickness as much as possible, and the pursuit to plate lithium metal in situ (in “anode-free” cells, which are more correctly described as “zero excess lithium metal” cells) without the use of an anode active material.^[4] Thus, the CAM type and content in the cell ultimately determine the maximum specific energy that the system can provide.

Moreover, the CAM contributes a significant proportion to the overall cell costs,^[5] hence the necessity of steady tailoring toward reduced costs and higher energy density. So far, CAM development has mainly targeted performance optimization with LEs in LIBs. For instance, cathode electrolyte interface (CEI) formation,^[6]

P. Minnmann, A. Bielefeld, R. Ruess, S. Burkhardt, E. Trevisanello, F. H. Richter, J. Janek
Institute of Physical Chemistry
Justus-Liebig-University Giessen
Heinrich-Buff-Ring 17, 35392 Giessen, Germany
E-mail: juergen.janek@phys.chemie.uni-giessen.de;
felix.h.richter@phys.chemie.uni-giessen.de

P. Minnmann, A. Bielefeld, R. Ruess, S. Burkhardt, E. Trevisanello, F. H. Richter, J. Janek
Center for Materials Research (ZfM)
Justus-Liebig-University Giessen
Heinrich-Buff-Ring 16, 35392 Giessen, Germany

 The ORCID identification number(s) for the author(s) of this article can be found under <https://doi.org/10.1002/aenm.202201425>.

© 2022 The Authors. Advanced Energy Materials published by Wiley-VCH GmbH. This is an open access article under the terms of the Creative Commons Attribution-NonCommercial-NoDerivs License, which permits use and distribution in any medium, provided the original work is properly cited, the use is non-commercial and no modifications or adaptations are made.

F. Strauss, S. L. Dreyer, T. Brezesinski, J. Janek
Battery and Electrochemistry Laboratory (BELLA)
Institute of Nanotechnology, Karlsruhe Institute
of Technology (KIT)
Hermann-von-Helmholtz-Platz 1, 76344 Eggenstein-Leopoldshafen,
Germany
E-mail: torsten.brezesinski@kit.edu

P. Adelhelm
Department of Chemistry – Electrochemistry
Humboldt-University Berlin
Brook-Taylor-Strasse 2, 14489 Berlin, Germany
P. Adelhelm
Joint Research Group Operando Battery Analysis
Helmholtz Centre for Materials and Energy
Hahn-Meitner-Platz 1, 14109 Berlin, Germany

H. Ehrenberg
Institute for Applied Materials (IAM)
Karlsruhe Institute of Technology (KIT)
Hermann-von-Helmholtz-Platz 1, 76344 Eggenstein-Leopoldshafen,
Germany

DOI: 10.1002/aenm.202201425

cracking of CAM particles,^[7] transition metal dissolution,^[8] and HF scavenging^[9] have been identified and extensively studied, and rational materials design has allowed to overcome these challenges.^[10] This resulted in today's state-of-the-art CAMs for LIBs, primarily referring to layered lithium metal oxides LiMO₂ (M = Ni, Co, Mn, Al, etc.). However, a transition from LIBs to SSBs is associated with different requirements for CAMs, which are rooted in the different properties of SEs (electrochemical stability, mechanical rigidity, etc.) as compared to LEs. Examples are different (electro-)chemical reactions at the electrolyte–CAM interface^[6,9,11,12] and increasing importance of (chemo-)mechanical processes^[13,14] or composite cathode fabrication.

The main types of solid lithium-ion conductors can be roughly divided into oxide-, sulfide-, halide-, and polymer-based SEs. Each of these material classes has distinct advantages and disadvantages, which have been summarized in several reviews elsewhere.^[15–22] For instance, oxide-based SEs possess a high (oxidative) electrochemical stability, preventing decomposition when in contact with (high-voltage) CAMs. However, their maximum ionic conductivity ($\approx 1 \text{ mS cm}^{-1}$ at room temperature [r.t.]) appears too low to enable fast charge/discharge kinetics, which can only be realized if the materials are sintered. Unfortunately, CAM/SE decomposition reactions take place at lower temperatures than required for proper sintering.^[23] In addition, their mechanical rigidity and brittle nature greatly complicate attaining and maintaining the required intimate contact with the CAM, especially when considering the volume changes occurring during cell cycling.^[21]

In contrast, polymer-based SEs possess favorable mechanical properties and can be processed in solution or molten form, which allows simple implementation into existing roll-to-roll processing lines for LIB fabrication. However, their ionic conductivities are yet too low for reasonable room-temperature operation, and limited oxidative electrochemical stability presents additional challenges during cell cycling. Nevertheless, polymer-based cells with LiFePO₄ (LFP) as CAM are available and used in public transportation.^[24]

The most prominent class of present-day SEs are sulfide-based materials, or in particular lithium thiophosphates, displaying exceptionally high r.t. ionic conductivities up to 25 mS cm^{-1} . They also have suitable mechanical properties (i.e., malleability and low Young's modulus), which makes them ideal candidates at first sight. However, they exhibit a narrow electrochemical stability window, and consequently, artificial protection layers avoiding direct contact with the CAM need to be implemented.^[21,25]

Halide SEs have recently regained great research interest, mainly owing to their high oxidative electrochemical stability, allowing their use together with unprotected CAMs. Apart from that, their mechanical properties allow moderate ionic conductivities (1 mS cm^{-1}) to be achieved in a cold-pressed state. In addition, they may also serve as a protective coating on the CAM surface, provided they do not react with the catholyte.^[26] As mostly rare-earth or other resource-critical metals are employed, their commercial use as catholyte is somewhat questionable.^[22]

Please note, that there are cell concepts using more than one SE.

To sum up, independent of the employed SE, a strong interplay between CAM and SE most likely requires a complementary design of both materials to achieve maximum

battery performance. In this perspective, we summarize specific issues regarding the application of inorganic CAMs in SSBs based on mainly sulfide and halide SEs. We elucidate the requirements of such CAMs to be addressed from a materials perspective and describe possible challenges and solutions. Building on this, we focus on proposed design principles toward improved CAMs, aiming to provide guidelines for rational CAM development for SSBs.

2. SSB Cathodes—Challenges

Composite cathodes in SSBs are generally composed of CAM and SE particles in combination with polymer binders and carbon-based additives, which improve the mechanical and electrical properties, respectively. In general, the fabrication of high-performance SSB cathodes presents challenges on different length scales, ranging from the micro- to the nano-scale which are related to the composite cathode, CAM particles, and interface between CAM and SE, respectively (Figure 1).^[27] Besides optimizing the composite cathodes on a microscale level, the CAM itself needs to be tailored for application in SSBs to be (chemo-)mechanically compatible with the SE. In the following, we describe the different requirements for the CAM and composite cathodes from materials and processing perspectives. Although various parameters related to the different materials (SE, binder, conductive additives) in SSB cathodes influence the cell performance, we focus on the particular design parameters of the CAM, as this material is the integral constituent.

2.1. Cathode Microstructure and Charge Transport

First of all, SSB cathodes should possess high ionic and electronic partial conductivities together with a high loading of CAM to remain within several tens of $\Omega \text{ cm}^2$ of internal cell resistance and maximize both, energy and power density.^[28] However, there is usually a trade-off between maximizing energy and power. For instance, a high content of CAM is necessary to increase the energy density of the cathode and in an ideal composite cathode, the CAM fraction approaches 100%. This goes hand in hand with a lower content of SE, which in turn increases the tortuosity of ionic conduction pathways and limits the attainable power density.^[29–33] Therefore, electrode engineering requires careful balancing of CAM volume fraction and electrode thickness. To date, experimental studies commonly use $\approx 50 \text{ vol\%}$ CAM fraction to ensure ionic percolation^[14,31,33–35] and geometrical models suggest an optimal composition in terms of active surface area between 60 and 70 vol% CAM fraction depending on the porosity in homogeneously distributed composites.^[36,37] We therefore anticipate, that, with tailored manufacturing techniques and liquid additives that reduce porosity and enable highly homogeneous particle distributions, commercial ASSBs, designed to provide high energy density, will target at least around 70 vol% CAM fraction. A detailed overview of experimentally achieved composite cathode loadings and the influence of kinetic transport limitations can be found elsewhere.^[38]

In contrast to cathodes employed in LE-based LIBs, porosity is detrimental to SSB cathodes and should be reduced to a

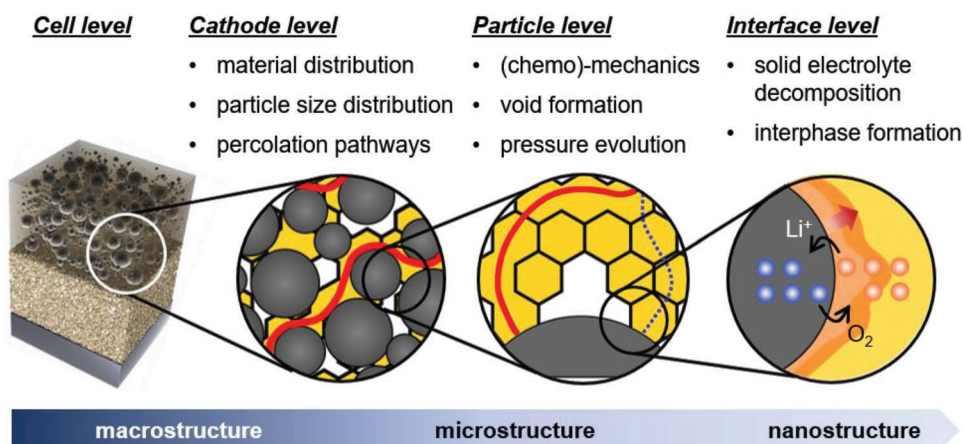


Figure 1. Schematic overview of the important processes occurring on different length scales in SSB cathodes, causing various challenges to the development of scalable fabrication processes and tailored materials properties.

minimum, as pores are neither electronically nor ionically conductive and negatively affect the charge transport.^[39] Apart from the conductivity, pores prevent active interface between SE and CAM and, depending on surface coverage, pore size, and distribution models, predict a significant increase in overvoltage.^[40] There is, of course, the possibility of introducing liquid ion conducting additives into the cathode to eliminate the pores, however, this concept leads to additional interfaces and needs further evaluation.

As a consequence, the charge-transport percolation, or in other words the ability to supply electrons and ions to all regions in the cathode, is a crucial condition when fabricating high-performance composite cathodes. Ionic and electronic percolation depends on several parameters, such as conducting-phase content,^[29–31,41,42] particle-size ratio,^[30,31,43,44] and processing conditions.^[34,45–48] Recent studies have shown that partial conductivities are suitable descriptors for the charge-transport percolation, and several experimental setups have been developed to determine the transport properties in different cathodes architectures.^[29,31,41,49,50]

The reader should note that SEs, different from LEs, possess their own microstructure, consisting of bulk and grain boundary, that can lead to ill-defined and non-uniform transport properties on the microscale (see **Figure 2**). Poorly conducting grain boundaries may further increase the “apparent tortuosity” of the ionic transport (as obtained from charge-transport measurements) beyond the “geometric tortuosity,” which only considers the respective distribution of phases. Thus, the SE and CAM particle microstructures are crucial for the electrochemical performance and have been studied from a modeling perspective alone or in combination with experimental works.

In general, the motivation for modeling composite cathodes for SSBs is driven by explaining experimental observations and, more importantly, providing guidelines on how to optimize the cathode microstructure. This involves the identification of the optimum composition of the cathode relevant parameters, such as particle-size distribution (PSD) of CAM and SE, required SE conductivity, and phase fractions of the

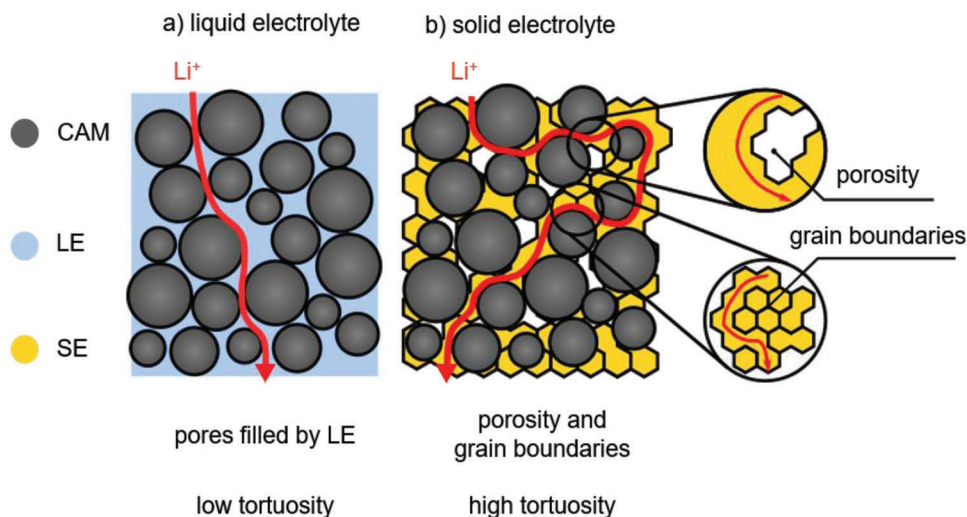


Figure 2. Comparison of composite cathodes using a) liquid- or b) solid-electrolyte. A liquid electrolyte can infiltrate the cathode and penetrate pores, leading to both, a uniform distribution of charge transport pathways and a low tortuosity for ion transport (red line in [a]). In the case of the solid electrolyte, residual porosity and grain boundary resistances result in much more tortuous transport pathways and a higher overall tortuosity (red line in [b]).

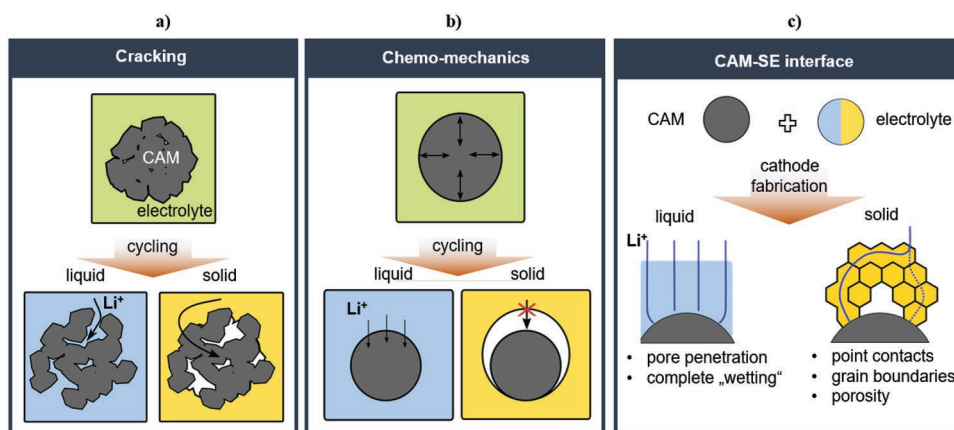


Figure 3. Schematic illustration of effects that come into play if changing the liquid electrolyte to a solid electrolyte. a) Cracking of CAMs induced by (chemo-)mechanical stress leads to reduced transport pathways in the case of a liquid electrolyte, because it can penetrate the newly formed pores. In case of a solid electrolyte, the transport pathways are increased in length. b) Large volume changes result in contact loss between CAM and SE and cause increased interface resistances. c) During cathode fabrication, a liquid electrolyte can penetrate the porous cathode and wet the free surface. A solid electrolyte is already part of the slurry before the cathode layer is fabricated. Although this may provide certain advantages in terms of reduction of processing steps, it is difficult to achieve intimate contact between CAM and SE, especially if the CAM possesses a complex surface morphology. Porosity and grain boundaries can affect the charge transfer and point contacts lead to current constriction and limit electrode kinetics.

respective constituents to achieve high energy and power densities while minimizing residual pore space. Most modeling studies rely on representing the cathode microstructure in voxels or simulate it using the finite-element method. To obtain a representative microstructure, voxel data are either directly imported from μ -computed tomography^[51] or focused ion beam scanning electron microscopy^[52] or reconstructed from SEM images.^[30,32,36,37] This allows to extract PSDs, particle shapes, or material distributions. In addition, fully synthetic microstructures are used to examine the impact of particular design parameters.^[30,36,37,45,53–57]

However, a challenge in the microstructure reconstruction is the high resolution that is required for binder and carbon additives, as these are much smaller in size and contrast to CAM and SE. Thus, most microstructure reconstructions do not take these components into account, with the exception of some recent studies reporting about the influence of the carbon black content in LFP/polyethylene oxide:LiTFSI composites,^[45,54] the microstructure of the carbon additive in $\text{LiNi}_x\text{Co}_y\text{Mn}_z\text{O}_2$ (NCM)/ $\text{Li}_6\text{PS}_5\text{Cl}$ (LPSCl) composites,^[58] and the effect of nitrile butadiene rubber and polyvinylidene-fluoride binders in NCM/LPSCl composites.^[32,37]

2.2. Chemo-Mechanics during Electrochemical Cycling

As all constituents of inorganic SSBs are solids and usually constrained by volume in the cell housing, (electro-)chemically driven volume or morphology changes during cycling have a profound effect on the performance and degradation. In the cathode, volume and/or morphology changes are in particular related to the CAM upon (de-)lithiation and are dependent on the state of charge (SOC). **Figure 3a,b** illustrates how common (chemo-)mechanical effects, such as interparticle stresses and CAM expansion/contraction, have to be taken into account when replacing a LE by a SE.

Since not all CAMs exhibit the largest volume change at the highest SOC, we focus on the maximum volume change ($\Delta V_{\text{max}}/V$) during cycling. Whereas conventional intercalation- or insertion-type CAMs mainly undergo volume changes in the range of several percent while maintaining the original crystal structure, conversion-type CAMs can undergo volume changes up to hundreds of percent, in addition to morphology changes due to the electrochemical conversion reaction. Please note, that volume changes are not necessarily isotropic^[43] and the resulting strain can differ significantly along different crystallographic axes, leading to massive anisotropic stress and mechanical damage. Thus, there is a strong current research interest to understand the effect of (chemo-)mechanical processes on battery performance and to find strategies to mitigate degradation mechanisms. For instance, the combination of thiophosphate-based SE (e.g., $\beta\text{-Li}_3\text{PS}_4$ [LPS] or LPSCl) and polycrystalline (PC) Ni-rich NCM CAM is highly attractive and often reported. This is mainly triggered by the high ionic conductivity of Li-thiophosphate SEs in combination with their malleability (low Young's modulus), which allows to accommodate (electro-)chemically driven volume changes during battery operation to a certain extent.^[21]

Such volume changes become more prominent if Ni-rich NCM or conversion-type CAMs are employed, leading to impedance increase and decreasing battery performance. However, modeling studies addressing (chemo-)mechanics remain largely elusive.^[59] In particular, the volume changes of the CAM during cycling can lead to interparticle cracking (for PC CAM) and pore formation between the SE and CAM particles, causing contact loss and increased tortuosity.^[13,14,48] In addition, it can be assumed that internal stress/strain generation in the cathode can cause cracking of the SE matrix (including the separator layer). This adversely affects the ionic and electronic percolation pathways, and ultimately results in poor electrochemical reversibility and capacity fading due to loss of contact to CAM upon prolonged cycling. While LEs can penetrate into these

pores and cracks,^[7] SEs are rigid and cannot do the same.^[13] On a laboratory cell scale, these effects have usually been compensated for by applying external pressures of a few to tens of MPa to the SSB. Clearly, such high pressures are not suitable for large-scale commercial applications.^[14,60] Consequently, it is important to find and develop materials combinations that allow to minimize or even avoid detrimental (chemo-)mechanical effects in SSB composite cathodes.

2.3. Interfacial Compatibility

In addition to the dominant role of (chemo-)mechanics, the interfacial compatibility between CAMs and SEs is another important issue. From a chemical perspective, the low chemical potential of lithium in the employed CAMs leads to oxidation of the SE. During oxidation, ionically poorly conductive phases are formed, for example, phosphites/phosphates, sulfites/sulfates, and polysulfides in the case of thiophosphate-based SEs. These narrow down transport pathways and cause an increased interfacial resistance, thereby impeding charge transfer.^[12,49,61] Oxidative SE decomposition can either be addressed via the implementation of stable SEs (i.e., oxides or halides) or through the application of a protective surface coating to the CAM, preventing direct contact with the SE. The primary function of a surface coating is to act as an electron blocking but lithium-ion conducting layer, so that the SE does not experience the low chemical potential of lithium in the CAM. However, sufficient electronic transport through the protective coating between the particles needs to be ensured to enable (de-)lithiation of the CAM. Moreover, if the coating itself is too brittle, it can lose contact to the CAM during cycling due to the accompanying volume/morphology changes. In addition, the application of a surface coating introduces new interfaces, namely SE/coating and CAM/coating interfaces, which may have detrimental effects on the charge-transport properties of the composite cathode.

Switching from thiophosphate- to oxide-based SEs comes along with different challenges, as oxide SEs are much more rigid, thus achieving and maintaining intimate contact with the CAM (and other electrode constituents) remains challenging (see Figure 3c) and often requires high-temperature sintering.^[23] In this regard, halide-based SEs (e.g., Li_3InCl_6 or Li_3YCl_6) may be a more suitable choice, as they combine high oxidation stability with favorable mechanical properties, but typically contain resource-critical and potentially costly elements.^[22] If only minor amounts of these materials are used in the form of nanoscale coatings their material cost is less of an issue.

In summary, interface engineering requires tailored approaches depending on the type of CAM and SE used and presents specific challenges for the materials development.

3. SSB Cathodes—Requirements and Solutions

As shown in Figure 1, SSB cathodes need to be tailored on different length scales, pertaining to challenges in the composite cathode, CAM particles, and interface formation between CAM

and SE. In the following, we describe the requirements going from the macroscale (cathode level) to the nanoscale (interface level), and outline possible optimization strategies for each level.

3.1. Cathode Level

To achieve high-performance SSB cathodes, careful balancing of the SE versus CAM content (and other additives) is required. Several experimental studies focused on tailoring these parameters, also addressing the charge transport and (chemo-)mechanical stability with the goal to increase cell performance.^[30,31] However, the fact that inorganic SEs possess their own microstructure (and PSD) implies that the SE and CAM PSD should be adapted to one another in order to achieve the highest possible packing density, thereby avoiding pore space and increasing energy density. It has been reported that the use of small SE particles (large CAM/SE particle-size ratio) in combination with spherical CAM particles is favorable for a high packing density.^[30,55,57] Moreover, for percolation modeling, experimental results indicate that NCM secondary particles with a diameter of 3–5 μm are beneficial for the interparticle connectivity, as they provide a sufficiently high specific surface area and many contact points with other NCM particles.^[36,37] Additionally, CAM fractions above 60 vol% may even enable carbon-free cathode composites if the electronic conductivity of the CAM is sufficiently high.^[31,36]

The most cost-effective way to fabricate SSB cathodes is to adopt already existing processes that are currently utilized in the production of LIBs, that is, slurry-based tape casting. However, new mixing strategies need to be developed, since the SE is usually already part of the slurry, and a uniform distribution of all electrode constituents after tape casting is required to maintain optimized charge percolation networks throughout the cathode.

A promising concept may be the application of gradient cathodes, in which a high electronic conductivity is achieved at the current collector and a high ionic conductivity is achieved at the separator side of the cathode.^[40,62] A gradient architecture compensates for the heterogeneity of the respective network resistance throughout the cathode cross section. Although the total charge flux through the cathode is constant at every distance from the separator and current collector, the resistance is smaller for ions at the separator, while the electrons experience a smaller resistance at the current collector side and vice versa.^[51,62] This can be understood in terms of a reaction zone model, where lithiation starts at the cathode side, at which the charge carrier experiencing the highest resistance is inserted. A detailed description is given by Usiskin et al.^[62]

Conductivity gradients can be achieved by varying the CAM volume content, and it may also be possible to use particles with different properties in different parts of the cathode. For instance, small particles with short diffusion pathways could be employed at the current collector side and larger particles at the separator side, so that ionic transport limitations will be mitigated. To further increase the rate capability, consideration of the above requirements may be useful in the design of CAMs. Another issue related to manufacturing is the amount

(and type) of binder needed to achieve mechanical integrity and to enable large-scale cell fabrication.^[37,46] To date, binder-containing cathodes have shown limited performance, as polymer binders block active (free) surface and conduction paths.^[35,63–65] There are approaches aiming at minimizing the binder content based on dry-processing using a PTFE-binder^[66] or by selective removal from the electrode via heat treatment.^[67] Dry processing has the advantage of excluding solvent from the production process, thereby eliminating the possibility of degradation reactions between CAM and solvent or SE and solvent. Additionally, high shear forces may be generated (extrusion) and could create sufficient contact points between the CAM and SE particles, provided the mechanical properties of the materials are tailored accordingly.

Another possibility is the liquid phase (melt) infiltration of the cathodes with subsequent SE crystallization, which can ideally result in a dense electrode.^[68] However, this approach requires SEs of low melting points and high ionic conductivity (yet to be discovered/synthesized).

As described previously, many parameters can influence the resulting performance. Thus, tailoring SSB cathodes via design-of-experiment approaches or comparable computation-aided methods is well suited to reduce the number of experiments needed.^[46]

3.2. CAM Particle Level

For the storage of lithium in the CAM, both electrons and ions need to be transported within a single particle, assuming that it is electronically and ionically well contacted, for example, by other CAM particles, conductive carbon (if added), and SE. It is essential to understand that the slowest process, either electronic or ionic transport, limits how much of the CAM is electrochemically addressed at a certain C-rate (in units of h^{-1}). Thus, the particle size L should be designed depending on the chemical diffusion coefficient \tilde{D}_{Li} of lithium as a neutral component (note that $\tilde{D}_{Li} \approx \tilde{D}_{ion}$ if the CAM is a predominantly electronic conductor) for a targeted C-rate, according to Equation (1), in order to achieve at least 83% of the theoretical specific capacity of a spherical CAM particle.^[69]

$$L \leq \sqrt{\frac{3\tilde{D}_{Li}}{C - \text{rate}}} \quad (1)$$

Figure 4 provides an illustration of the particle size calculated from Equation (1) for the \tilde{D}_{ion} in NCM and \tilde{D}_e in LFP exemplarily. For conversion- and spinel-type materials, it is difficult to obtain \tilde{D}_{Li} , because most of these materials undergo several phase transitions, and two phases are present over a large range of SOC. We would like to note though that \tilde{D}_{ion} in spinel-type materials should be higher than that of layered NCM CAMs.^[70] Evidently, even for materials with high \tilde{D}_{Li} , such as NCM, the particle size should not exceed more than a few micrometers if high C-rates are to be achieved.

In this regard, small CAM particles are beneficial to achieve high capacities at a high C-rate. However, an optimum particle size exists, as too small particles compromise ionic partial conductivity and ionic percolation on the cathode level.^[30,37,72] This

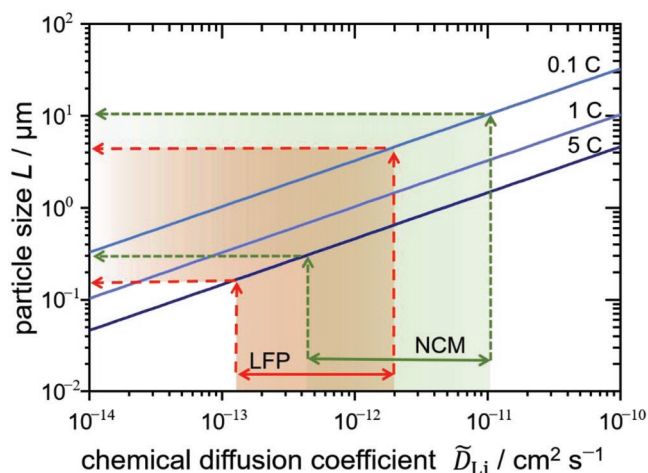


Figure 4. Maximum particle size according to Equation (1) for a C-rate of 0.1, 1, and 5 C depending on the range of the respective diffusion coefficient (colored areas). For NCM CAMs, the diffusion coefficient for ions was considered,^[7] while for LFP and conversion-type materials, the diffusion coefficient for electrons was considered,^[7] because they are mostly poor electronic conductors.

is especially critical if also degradation at the CAM|SE interface is taken into account, which is more detrimental in the case of small particles due to the larger contact area.^[37,49]

As mentioned above, the initial particle size of a certain CAM does, in most cases, change during cycling. The changes in lithium concentration within the CAM upon charging and discharging lead to volume changes of the primary particles that predominantly expand (e.g., LiCoO_2 [LCO]) or shrink (e.g., Li_2S or NCM) with delithiation. The volume changes are typically in the range of a few percent for intercalation-type CAMs, whereas for conversion-type CAMs, the volume changes are much larger, depending on the cell chemistry involved. Based on the electrochemical reaction formula during discharging, a theoretical volume expansion of 78% and 65% can be calculated for the conversion-type CAMs sulfur and iron disulfide, respectively. Although the relative volume change is independent of the particle size, it has to be taken into account that smaller particles show smaller absolute changes in L . Figure 5a shows the absolute change of the particle radius r (with $r = L/2$) as a function of the initial particle radius r_0 for several CAMs. For smaller particle sizes, smaller changes occur, which may be accommodated more easily by SE deformation. Yet, it is unclear to which extent SEs are capable of compensating the CAM volume change.

Importantly, the volume changes are correlated to the lithium concentration within the CAM, so that lithium concentration gradients, typically generated at high C-rates, as well as the anisotropy of the volume changes, lead to mechanical stress. This can result in the formation of cracks either between different grains in PC CAMs or within individual single-crystalline CAM domains. Such cracks within the CAM increase the electronic tortuosity throughout the composite cathode, since they effectively block electronic charge transport and increase the length of the electronic pathway. The increase in electronic tortuosity is even more pronounced if CAM particles close to the current

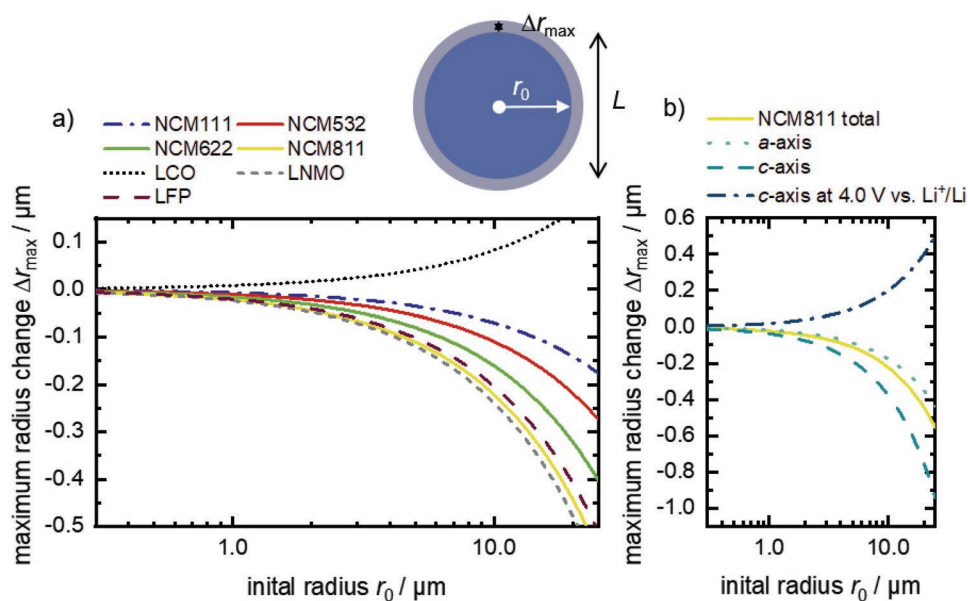


Figure 5. a) Calculated maximum radius change of spherical CAM particles as a function of the initial particle radius r_0 .^[14,73–75] The absolute maximum volume change is much smaller for smaller particle radii, and the differences between different types of CAMs become less pronounced. b) Deconvolution of the total volume change of NCM811 into c - and a -axis changes.^[76] The c -axis first expands up to a potential of 4 V and subsequently contracts. The differences in the c - and a -axis change lead to internal stress and may cause anisotropic volume changes of SC CAMs. For conversion-type CAMs, more elaborate calculations would require knowledge of the phase nucleation geometry and are beyond the scope of this work.

collector crack, as this is accompanied by contact loss between CAM and current collector.

To mitigate interparticle cracking, the development of single-crystal (SC) CAMs appears to be a promising approach.^[77] Nevertheless, SC CAMs still show an overall volume change during (de-)lithiation and will not change volume isotropically, due to different crystallographic orientations of the facets and the anisotropic changes in the a - and c -axis. Please note that the c -axis initially expands during delithiation due to increased Coulombic repulsion of the oxygen layers. At a certain Li-concentration (corresponding to around 4 V vs Li^+/Li) these layers collapse, and the c -axis exhibits substantial contraction (see Figure 5b). The contact loss along certain facets could be much more severe, than expected from the total volume change. Hence SC CAMs may not necessarily be an ideal solution to the chemo-mechanical problems in SSBs, unless the particle shapes can be tailored in a controlled way.^[78] However, this point is quite unclear so far and needs further evaluation.

Thus, multiple other strategies have been developed, each with its own advantages and disadvantages. First, the use of zero- or low-strain materials eliminates the volume changes during battery operation directly. For instance, NCM CAMs showing virtually zero volume changes during charge/discharge have been developed via rational tailoring of the transition metal composition. This results in almost no pressure evolution on a cell level during cycling.^[79] However, one again has to consider that such materials do undergo anisotropic volume changes along different crystallographic directions as mentioned above, yet these result in zero net changes upon (de-)lithiation. Thus, on the microscale, (chemo-)mechanical separation between SE and CAM may still occur.^[79] Alternatively, the overall balancing of volume changes on the cell level has also

been achieved by blending CAMs that shrink with CAMs that expand during delithiation (e.g., $\text{LiNi}_{0.8}\text{Co}_{0.1}\text{Mn}_{0.1}\text{O}_2$ [NCM811] and LCO)^[14] or by combining expanding anodes with shrinking cathodes and vice versa.^[80] However, in both aforementioned cases, the development of quasi zero-strain cathodes comes at the expense of decreased Ni content and thus, specific capacity.

Recently, it has been demonstrated that pressure changes and secondary particle fracture in SSBs can be mitigated via the application of “full-concentration gradient” NCM CAMs, which possess radially oriented rod-shaped primary crystallites, unlike conventional NCMs.^[81] Apart from addressing pressure evolution through designing the CAM itself, this issue may be counterbalanced by the introduction of certain amounts of suitable polymer binders and/or additional polymer SEs into the cathode to buffer pressure changes during cycling and maintain mechanical integrity.

3.3. Interface Level

Although already several CAM design strategies to minimize detrimental (chemo-)mechanical effects in SSBs have been developed, the interface formation, that is, SE degradation remains problematic. To prevent side reactions that form high-impedance interphases, a common approach is the application of a protective surface layer to the CAM particles, usually with a thickness in the nanometer range. In principle, the primary requirement for such coatings is to act as an electron-blocking but ion-conducting layer while having high oxidative stability. To this end, various lithium transition metal oxides (e.g., LiNbO_3 , LiTaO_3 , and Li_2ZrO_3) have been studied in the past, and SE degradation could be strongly suppressed, ultimately

leading to increased performance and long-term cycling stability.^[64,82–84] Although usually specific coating compositions are aimed for, it has been recently shown that especially for Ni-rich NCM CAMs this may differ in reality. For instance, surface residuals, such as Li_2CO_3 and LiOH , are known to be present on NCM CAMs, which are eventually incorporated into the coating and may play an important role in stabilizing the as-formed interface.^[85] Moreover, one has to consider that the volume changes of CAMs upon charging and discharging not only create mechanical stress in the CAM (and on the cell level), but also exert similar stress to the interface between CAM and coating. Thus, the contact between coating and CAM may be deteriorated with continuous (de-)lithiation so that the protective function decreases or even vanishes. Additionally, interfacial reactions can also cause significant volume changes due to the different specific volumes of educts and products. If the volume changes resulting from such interfacial reactions are sufficiently pronounced, they can even lead to contact loss between CAM and SE.^[86] As a result, specific coating chemistries and tailored synthetic procedures need to be developed for different CAM types. A detailed discussion about the functionality of CAM coating properties can be found elsewhere.^[25] Please note, that recently the potential of halide SEs and polymers as protective surface coatings has been evaluated.^[22,87]

To conclude, different factors have to be considered when designing the CAM and CAM PSD, which are summarized in **Figure 6**. Charge transport percolation, diffusion pathways inside the CAM, and active interface area are critical parameters which are influenced by the particle size distributions of CAM and SE. To increase the cathode performance, these parameters need to be adjusted complementary. While smaller particles offer the advantage of percolation and shorter diffusion pathways, their high specific surface area can create additional challenges. Therefore, tailored PSDs of CAM and SE are necessary, and these PSDs may be different for every system/combination.

4. Design of Individual CAM Types

In the following, we highlight current research trends for the application of different types of CAMs in SSBs. In particular, we compare layered lithium transition metal oxides (LiMO_2), polyanionic LFP, spinel-type $\text{LiM}_2\text{O}_4/\text{LiNi}_{0.5}\text{Mn}_{1.5}\text{O}_4$ (LMO/LNMO), and conversion-type materials (M_aX_b) and consider the different reaction mechanisms. Moreover, we discuss advantages and limitations of design methodologies for each type of CAM regarding their application in SSBs and propose additional solutions, which go beyond the state-of-the-art.

4.1. Intercalation-Type (Layered) CAMs

In intercalation-type materials, lithium is stored in between layers typically consisting of transition metal and oxygen ions, similar to cars being parked in a multi-level parking garage. During the intercalation process, lithium ions enter the material from SE contacts and the added positive charge is immediately compensated by transfer of an electron from electronic

contacts, effectively leading to the incorporation of a neutral lithium atom. After transfer, lithium diffuses inside the CAM toward the center of the material due to its concentration gradient. During deintercalation, the process takes place in reversed direction. We like to note that this process needs to be described as “chemical diffusion” of lithium, that is, the diffusion coefficient \tilde{D}_{Li} includes kinetic (diffusion coefficients of ions and electrons) and thermodynamic contributions (thermodynamic factor). It is a nonlinear function of the lithium concentration.^[88,89]

Intercalation-type layered lithium transition metal oxide CAMs with the general formula LiMO_2 find widespread application in LE-based LIBs and are widely investigated to be employed in SSBs. Usually, mixed transition metals are introduced referring to NCM or NCA materials (e.g., NCM811 or $\text{LiNi}_{0.8}\text{Co}_{0.15}\text{Al}_{0.05}\text{O}_2$). The strong interest in this class of materials is mainly driven by their superior volumetric energy density over other CAMs. However, they display two main issues when it comes to their application in SSBs. First of all, they operate at potentials high enough to cause the electrochemical oxidation of many highly conductive (mostly thiophosphate) SEs, leading to the progressive growth of a resistive CEI.^[85,90] Second, they show relatively large volume changes upon (de-)lithiation, causing mechanical degradation of the secondary particles and leading to severe contact loss between CAM and SE.^[14,86,91] Additionally, NCM materials exhibit anisotropic expansion and contraction along the crystallographic c and a directions and these unit cell distortions are creating significant internal stresses. Thus, design strategies for this class of materials need to minimize 1) the interfacial reactivity in contact with the SE and 2) mitigate detrimental (chemo-)mechanical effects.

In the first case, protective coatings mostly based on lithium-containing oxides with Nb, Ta, Ti, Zr, Al, or B are employed to alleviate (electro-)chemical oxidation of the SE via preventing direct contact between CAM and SE.^[25,64,83,92–97] Protective surface coatings are especially relevant when using SEs with a narrow stability window, such as lithium thiophosphates. It should be noted that thiophosphate-based SEs generally tend to react with oxides (including the coating itself), due to the formation of energetically favorable phosphite/phosphate and sulfite/sulfate compounds, and chemical reactions are not completely avoided by protective CAM coatings.^[93] However, coatings with sufficiently low electronic conductivity can shield the low chemical potential of lithium in the CAM, which attenuates the oxidation of the SE and has been shown to be beneficial to the cathode stability. While usually simple stoichiometric compounds have been targeted for the coating, it has recently been shown that the chemical composition obtained after the coating process may actually deviate from the targeted composition. Specifically, Ni-rich layered oxides show a natural presence of surface impurities, such as Li_2CO_3 and LiOH . Although contradictory results have demonstrated that Li residuals alone are already capable of somewhat stabilizing the SE/CAM interface,^[84,98–102] they can be incorporated into the coating during preparation and may be advantageous when included in a controlled manner.^[82,84,85,98,101] This might also be the reason why nominally binary oxide-based coatings show beneficial properties if applied to NCM-type materials for SSB applications, as

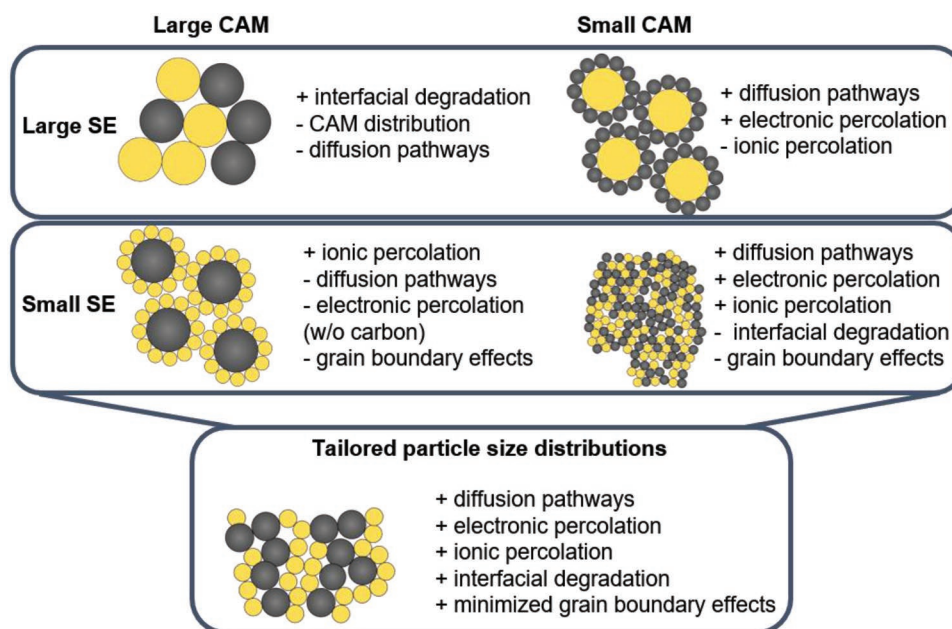


Figure 6. Influence of CAM and SE particle size on the different aspects of requirements for SSB cathodes. CAM particle size determines the properties on all three levels of composite cathodes and is an important design parameter for optimum cyclability in terms of kinetics and stability.

such oxides do not show significant lithium-ion conductivity.^[103] Moreover, post processing of, for example, NCA can lead to significant improvement in performance, further emphasizing the role of surface residuals in Ni-rich layered oxide CAMs.^[104] Apart from the development of customized coating compositions, the micro- and/or nano-structure of the coating itself may also play an important role.^[105] This has been evidenced, among others, through the preparation of a high-quality coating on a Ni-rich NCM consisting of a carbonaceous (Li_2CO_3) layer and a ZrO_2 nanocrystal mono or bilayer. This kind of coating helped to improve considerably the cycling performance of thiophosphate-based SSBs.^[106]

However, note that electronic percolation throughout the composite cathode still needs to be maintained by either plastic deformation of the coating during electrode calendaring or incomplete coverage of the coating with the combination of small CAM particles and (surface tailored) conductive carbon additives.^[58] Besides the tailoring of the coating composition, the deposition technique itself will have a profound effect on the resulting CAM performance. Simple sol-gel approaches involving alkoxides are widely used in literature. However, the coating quality in terms of conformity and surface coverage is rather poor. Here, atomic layer deposition (ALD) may be an alternative route to produce coatings of uniform thickness and composition at the expense of costly equipment and processing. Combining the advantages of both sol-gel and ALD techniques, it has been demonstrated that by using highly reactive precursors in a liquid-phase process, ALD-like surface coatings can be achieved in the case of Al_2O_3 .^[107,108] Thus, we believe that properly adjusting precursor reactivities and taking into account the composition, reactivity, and functionalization of the CAM surface may lead to the development of simple, cost-effective approaches toward high-quality protective coatings.

On top of the (electro-)chemical instability at the SE/CAM interface, several irreversible changes take place in the CAM itself during (de-)lithiation. These involve detrimental phase transformations primarily at high SOC (e.g., from active layered into inactive rock-salt type structure) and (chemo-)mechanical degradation, such as contact loss and cracking of secondary particles. The aforementioned structural transformation is accompanied by the release of molecular oxygen, which can further react with the SE.^[85,109,110] Such side reactions can additionally contribute to the buildup of a resistive SE/CAM interface and cause an increase in overpotential, which progressively lowers the cell performance. Traditionally, coating of CAM is pursued for mitigating both LE decomposition and rock-salt formation. However, in recent years, the focus has shifted toward bulk and surface doping, thereby preventing deleterious phase transformations via crystal lattice stabilization.^[111,112] This can be achieved by substituting the redox-active transition metals with other redox-inactive elements, with NCA being the most prominent example.^[113] As the substituent cannot be oxidized, some of the lithium in the structure cannot be extracted, thus preventing the formation of the rock-salt phase and lattice oxygen release.^[113,114]

Apart from phase transformations, the (chemo-)mechanics of layered oxide-based CAMs during (de-)lithiation may cause detrimental effects. Pronounced volume changes occur when lithium is removed from the layered structure (e.g., $\Delta V_{\text{max}}/V \approx -5\%$ for NCM-811 at 4.3 V vs Li^+/Li).^[76] This can lead to contact loss between CAM and SE or cracking of secondary CAM particles, which ultimately results in longer transport pathways and lower capacities (see Equation (1)).^[86,91] In the case of LE-based LIBs, secondary particle fracture is not as harmful as for SSBs, because the LE can penetrate into the newly formed voids. Cracking even shortens the lithium-diffusion pathways and allows utilizing the full capacity of large

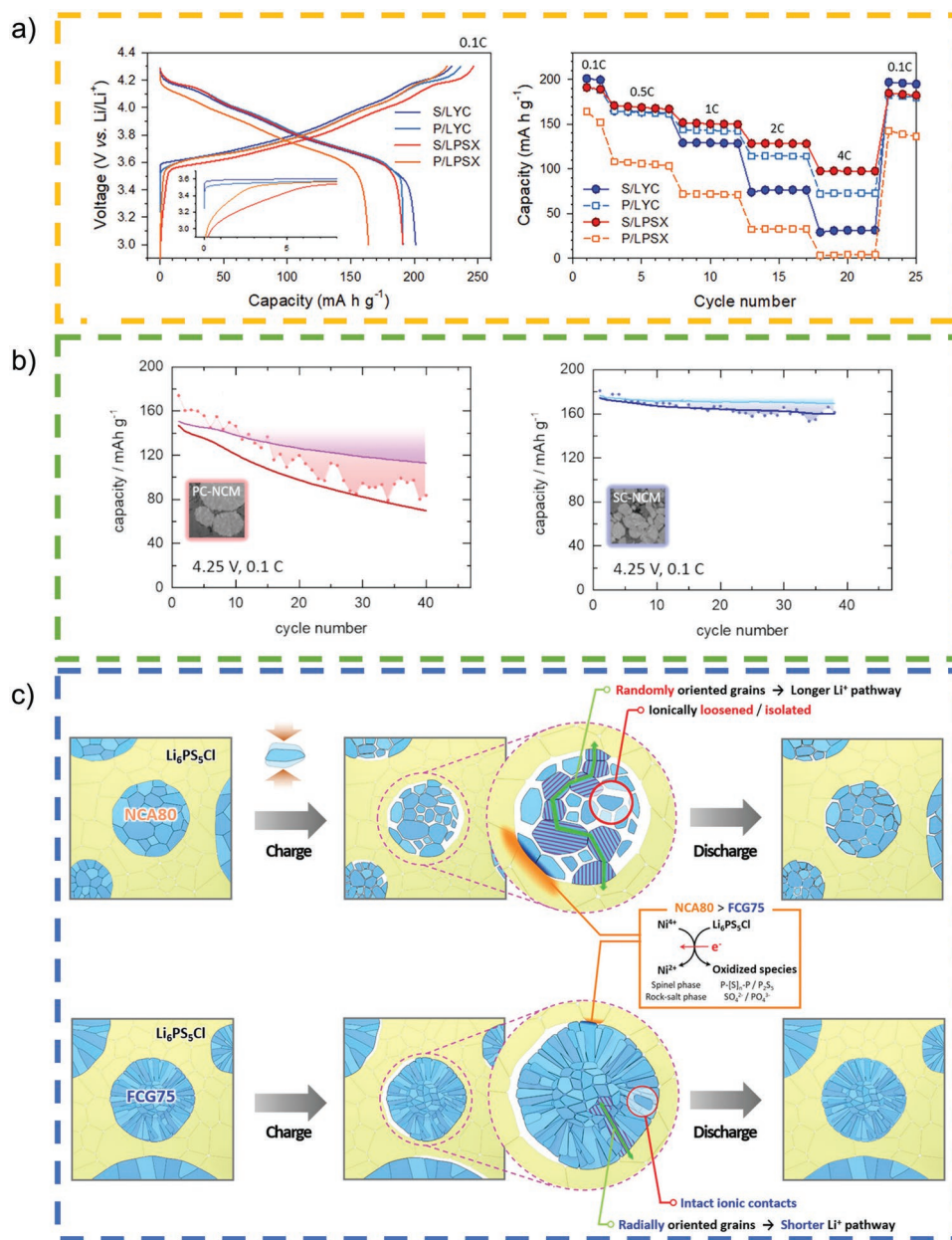


Figure 7. Strategies to overcome chemo-mechanical challenges in CAMs for SSBs: a) Influence of the choice of solid electrolyte (LYC = Li₃YCl₆, LPSX = Li₆PS₅Cl) on the performance of NCM with PC (P) or SC (S) particles. Reproduced with permission.^[86] Copyright 2021, John Wiley and Sons. b) Influence of particle cracking on the cycling stability of SC and PC NCMs. Reproduced under terms of the CC-BY license.^[91] Copyright 2021, The authors, published by IOP Publishing. c) Mitigating CAM particle cracking by the use of tailored "full concentration gradient" (FCG) CAM particles with rod-shaped crystallites. Reproduced with permission.^[81] Copyright 2019, John Wiley and Sons.

(micrometer-sized) secondary CAM particles, which deliver lower specific capacities in SSBs.^[7,13]

Addressing the issue of (chemo-)mechanical degradation, several strategies have been developed. One recently pursued approach is the development of SC NCM materials (Figure 7a,b).^[86,91] Here, the major goal is the application of CAMs with monolithic grains. It is worth noting, that most of the investigated SC NCM materials do not exhibit a pure single crystalline morphology, but rather consist of agglomerates of micrometer-sized monolithic grains, as synthesizing fully separated single crystals is very challenging.^[104,115,116] In

theory, such SC NCM CAMs should prevent particle cracking but still be susceptible to loss of contact with the SE as a result of the unit-cell volume changes during (de-)lithiation. Indeed, several reports have shown the favorable mechanical behavior of SC CAMs in SSBs, leading to much improved morphological integrity and better capacity retention. Ni fractions of up to 88% with high capacity retention (96.8 % after 200 cycles)^[86] as well as high specific capacities (210 mAh g⁻¹)^[117] have been realized in SSBs employing SC CAM so far. With a further increase in Ni content and additional facet engineering, even higher performance can be expected.^[118,119]

The increased performance of SC CAMs is sometimes also explained by the smaller particle size compared with conventional PC secondary particles.^[36] However, using PC CAMs with equally small secondary particles, which then have an even higher specific surface area, similar specific discharge capacities, and performance were found for NCM811, when setting the upper cutoff voltage to 4.15 V versus Li⁺/Li. Only when it was increased to 4.35 V, thereby inducing secondary particle fracture, SC CAM outperformed the PC counterpart.^[120] At the same time, depending on the mixing procedure and choice of SE, the use of small particles may lead to non-uniform spatial distribution of CAM in the cathode, resulting in SC particles touching and inducing strain on each other, thereby negating any initial benefits.^[86] However, the particle size of SC materials can be controlled to some extent during the synthesis (and independently from the precursor particle size), thus optimization of both CAM size and CAM/SE particle-size ratio, as discussed before, can be achieved.^[121]

The design of a cathode composite should also consider the excess lithium inventory required to compensate for side reactions at the anode. In LIBs, the capacity lost in the first cycle, linked to the kinetic limitations of the CAM at the end of discharge, is effectively used for the formation of the SEI. However, whether or not lithium excess is needed in SSBs depends greatly on the anode design. When such a compromise is not necessary, the particle size of the CAM can be tailored for high Coulomb efficiency in the first cycle. As previously discussed, by reducing the particle size of the layered oxide CAM, both a higher active surface area and shortened lithium diffusion length can be achieved, thereby improving the discharge capacity. Nevertheless, surface doping efforts toward structural stabilization have proven to be successful only for PC materials, with scarce literature about similar improvements for SC ones. Here, the required high-temperature processing might pose some challenges, with dopant diffusion inside the particle practically preventing selective surface modification.

Apart from the development of SC NCM CAMs, other crack mitigation strategies, such as the aforementioned gradient particles with rod-shaped primary particles (Figure 7c), have also been pursued.^[81] Here, the primary crystallites are preferably grown along distinct crystallographic directions to counterbalance the anisotropic volume changes during (de-)lithiation and avoid cracking of the NCM secondary particles. Although contact loss between CAM and SE still occurs to some extent for this example, the overall cell pressure evolution and loss of active material are strongly reduced, thus improving the cell performance.

4.2. Insertion-Type CAMs

For insertion-type CAMs, lithium is stored on free lattice sites located within a rigid (3D) crystal framework, offering Li-ion conduction via vacancies and interstitial sites. Usually, the insertion/extraction of lithium causes minimal shrinkage or expansion of the host structure, hence a high structural stability of such CAMs during operation can be anticipated. In principle, two kinds of insertion-type CAMs have been investigated in SSBs so far, namely LFP (olivine structure) and LMO or LNMO

(spinel structure). Due to their respective operating voltage of 3.5 and 4.5 V versus Li⁺/Li, a much more severe SE decomposition occurs for LNMO, the higher voltage CAM. Although the redox potential of LFP seems suitable to be employed with most SEs without severe interfacial degradation, the main drawback lies in its intrinsic low electronic conductivity (in the range of 10⁻⁹ S cm⁻¹ at r.t.). Thus, LFP is usually carbon coated or mixed with a large fraction of conductive additives to ensure sufficient electronic percolation, which creates issues in SSBs. Adding carbon has been shown to deteriorate cycling performance, especially in the case of thiophosphate-based SSBs.^[58,122–124] This issue might be the reason why reports about LFP in inorganic SSBs are scarce, and LFP is usually combined with polymer-based SEs. Nevertheless, it has been claimed that the electronic conductivity of LFP can be significantly increased via doping on the Fe site (up to 10⁻³ S cm⁻¹ at r.t.).^[125] Yet, the performance of such doped CAMs in SSBs remains elusive. We believe that the intrinsically low partial electronic conductivity of polyanionic electrode materials may present the biggest hurdle toward their implementation in SSBs. Moreover, the application of LFP (or derivatives) in SSBs would most likely be cost-driven, as especially the gravimetric energy density is rather low compared to state-of-the-art NCM CAMs.

However, higher energy densities could possibly be achieved through the implementation of high-voltage spinel lithium manganese oxide-based CAMs (e.g., LMO or LNMO), which offer a redox potential of up to 4.7 V versus Li⁺/Li. Nevertheless, according to published research data, it seems challenging to realize this potential advantage. Using LNMO together with, for example, lithium thiophosphates causes severe SE degradation and poor capacity retention.^[126–129] To prevent such detrimental side reactions, conventional protective surface coatings have been applied to LNMO but without significant performance improvement. Normally, a specific discharge capacity of ≈80 mAh g⁻¹ specific discharge capacity is achieved in literature for surface-protected LMO/LNMO CAMs in SSBs, which is relatively low compared to the theoretical specific capacity (147 mAh g⁻¹ for LNMO). A recent study comparing different lithium transition metal oxide surface coatings on LNMO has shown that depending on the coating chemistry, an improvement over the pristine CAM can be achieved.^[130] Additionally, the use of halide SEs, which offer a high oxidation stability may be another suitable alternative to enable high voltage CAMs such as LMO/LNMO in SSBs.

Achieving SSB performance close to the theoretical capacity of LMO-type CAMs needs further engineering on several parameters, which are generally important in the case of SSBs, such as the particle size, intragranular porosity, or the application of a protective surface layer.

4.3. Conversion-Type and In Situ Formed CAMs

Conversion-type CAMs undergo distinct phase changes during (de-)lithiation, that is, phases with very different physicochemical properties occur during cycling. This is different from intercalation- and insertion-type materials, which maintain their structure, that is, their overall properties remain similar during cycling. The key advantage of conversion-type CAMs

(which, except for elemental sulfur, can be described as by M_aX_b , M: transition metal, X: anion) is their higher specific capacity while on the downside they show much larger volume changes. Typical values are several hundred mAh g^{-1} and several tens to a few hundred vol%, respectively. Additionally, the redox potential increases with the ionicity of the bond, that is, transition metal fluorides have the highest redox potentials. Among the transition metals, copper compounds show the highest redox potential. The “upper limit” is therefore found for CuF_2 , which theoretically has a redox potential of 3.53 V versus Li^+/Li , that is, slightly below NCM CAMs. However, because the conversion reaction involves the formation of intermediate and amorphous phases, it is only partially reversible and typically (but not always, see below) leads to a nanoscopic structure comprising transition metal nanoparticles dispersed in an amorphous Li_xX matrix. Structural characterization of this nanoscopic/amorphous structure and theoretical description are more challenging than for other CAMs. Even for seemingly simple compounds, like FeF_3 , FeS_2 , CuS , Mn_3O_4 , or MoS_2 , the reaction mechanisms are still under debate.^[131–136] Moreover, electrolyte decomposition takes place, leading to thick surface films and initial Coulomb efficiencies typically below 75%. Overall, the appearance of intermediates and the formation of nanoscopic/amorphous structures along with electrolyte decomposition lead to more sloping voltage profiles and often large voltage hysteresis (low energy efficiency).^[137–140]

A challenge for using conversion-type CAMs in SSBs is often their poor electronic or ionic conductivity. Thus, conductive percolating networks cannot be created by the CAM alone, and additionally, the transport within the CAM particles limits the charge-transport kinetics. Hence, CAM nanosizing and addition of large amounts of conductive additive(s) are typically required, both of which is detrimental to the electrode capacity if SEs with a narrow electrochemical stability window are used.^[41] Nevertheless, the use of SEs may overcome specific limitations of particular conversion reactions, such as the electrolyte instability or polysulfide solubility in the case of Li_2S or S_8 as CAMs. The confinement of the active material in a SE may also help to mitigate undesired particle growth during cycling. However, at the same time, the mechanical properties (hardness, volume expansion, etc.) become more important when designing conversion-type CAMs for SSB applications.

Several conversion-type CAMs have been explored for SSBs in the last years among FeS_2 , CuS , and S_8 . FeS_2 (pyrite) has a theoretical specific capacity and cell voltage of 894 mAh g^{-1} and 1.84 V, respectively. Similar to LE-based LIBs, the CAM performance in the experiment deviates from this ideal case.^[141] Clear steps in the voltage profile are only observed at elevated temperatures or at very small currents, for example, using polymer electrolytes (120 °C)^[142] or inorganic glass electrolytes (20–60 °C).^[100,143] While there has been dispute over the active phases during cycling, Yersak et al. demonstrated that the application of SEs leads to significant improvements in cycle life compared to LEs.^[100] The same authors also confirmed the formation of FeS_2 upon charging (along with non-stoichiometric FeS_y and sulfur), that is, a multiphase mixture is formed. At r.t., cell cycling still shows an issue due to high polarization although nanosizing of the active material can be a strategy to mitigate this.^[144] The need for particularly careful electrode

optimization, for example, regarding particle size in the case of FeS_2 , is also obvious from its comparably high Mohs hardness (6.0–6.5) and large electrode expansion during initial lithiation (163%).

CuS (Covellite) is a naturally occurring mineral. Special aspects of using CuS as electrode material are the complex $Cu-S$ phase diagram, which shows several non-stoichiometric compounds, such as $Cu_{2-x}S$. Compared to FeS_2 , the energy density of CuS is lower, but it is much softer, shows a slightly higher cell voltage, and a smaller volume expansion. A key advantage is that copper sulfides are electronically conductive (e.g., 870 S cm^{-1} at r.t. for CuS)^[133] and also show a high conductivity for Cu ions,^[145] which can help to minimize the amounts of SE and conductive additives required in the SSB cathode. Among the compounds tested in conversion reactions, CuS is quite unique in that the material undergoes a displacement reaction, in contrast to the nanostructure formation seen for other conversion electrodes. This means that macroscopic copper forms during lithiation of CuS . This has been described in LE-based LIBs by Debart et al.^[132] but recently also found to occur in SSBs.^[146] In SSBs with LPS as SE, Aggunda et al. found a network of μm -sized Cu crystals after discharge, which were even visible by eye.^[146] No conductive additive was used in this study.

Both metal sulfides discussed here show a mixed cationic (Fe/Cu) and anionic (S) redox chemistry. This is naturally different for pure sulfur, which is another promising conversion electrode for SSBs and has drawn great attention in the last years.^[147–150] The main reason is the low cost of sulfur and its high theoretical specific capacity of 1672 mAh g^{-1} , providing a high specific energy (the advantage is less considerable with respect to volumetric energy density). The use of SEs prevents the well-known dissolution of soluble polysulfide intermediates that cause a shuttle mechanism and electrode degradation in cells with LEs. The lack of dissolution/precipitation processes during cell cycling also leads to a simpler, in this case very flat voltage profile of SSBs, compared to their analogues with LEs. In fact, experiments indeed show a flat voltage profile in agreement with the phase diagram (Li_2S being the only stable binary lithium-sulfur compound). The main challenge of using sulfur in SSBs is, next to the volume expansion of around 80%, that both the charge (sulfur) and discharge (Li_2S) products are electronic insulators. This requires nanosizing and the addition of large amounts of conductive additives compared to other conversion materials.

Another approach is to combine sulfur and transition metal sulfides in a single electrode, that is, using $CuS+S_8$ or FeS_2+S_8 composites as electrodes. This approach has been realized in 2003 already by Hayashi et al.^[151] but is nowadays more frequently applied.^[152–154] Overall, the large number of conversion reactions and possible combinations in composite electrodes provide a versatile playground for developing conversion-type electrodes for SSBs. The three cases discussed here (FeS_2 , CuS , and S_8) are especially appealing, as they show unique properties. Few grave challenges, however, apply to most of the conversion reactions. First, their large capacities are intrinsically coupled to large volume changes that need to be considered in the electrode and overall cell design. The mechanical properties of the CAM, SE, and composite probably need to be tailored

accordingly. Second, in many cases, nanostructures form during cycling, which show a high surface area that can trigger severe side reactions with the SE, thus causing fast capacity decay. Third, in most studies on conversion electrodes, cells are assembled in the charged state. This means that lithium (or a lithiated compound) is needed as a counter electrode, which is a clear drawback for commercialization. It is therefore important to draw more attention on lithiated conversion-type CAMs, however, identifying and synthesizing such compounds is not trivial.

It is worth noting, that several other CAMs are being explored in SSBs. In a recent approach, a lithium argyrodite SE has been used in a simple SE/C composite as a precursor for the in situ formation of redox active sulfur and phosphorus phases, thus achieving another type of two-element redox activity.^[155] Additionally, organic CAMs, in which multi-electron transfer reactions occur during (dis-)charging, have been used recently in SSBs.^[156–158]

5. Guidelines in Short

So far, we have identified and reviewed several aspects that play a role in composite cathodes for SSBs, and have shown how these affect different types of CAMs. In the following, we summarize the essential aspects that need to be considered when designing CAMs on different length scales for SSBs.

5.1. Cathode Level

Effective electronic and ionic percolation as well as full active material utilization are of prime importance—often expressed by partial effective conductivities. CAM/SE PSDs and particle shapes should allow ideally close packing. For optimal charge transport, it is crucial to reduce porosity to a bare minimum and to increase the effective ionic conductivity of crystalline SEs through grain boundary design. Gradient cathodes may require different CAMs and/or CAM particle sizes at the current collector and separator side. In an ideal case, CAM and SE particle size and distribution are designed simultaneously.

5.2. Particle Level

Particle cracking and internal porosity in the CAM have to be avoided. Particle sizes and shapes have to be adjusted to the electronic and ionic transport properties, which ultimately determine the optimum size. Gradient particles may show benefits with respect to avoiding (chemo-)mechanical degradation. Doping grain boundaries may be an effective strategy to achieve more stability and/or adjust kinetics.

5.3. Interface Level

A stable CAM/SE interface has to be achieved, either by coating, by the formation of a native passivating CEI, or both. Coatings should be primarily lithium-ion conducting but allow sufficient

electronic percolation within the electronic conduction pathways through the cathode generated by the CAM particles and, if required, conductive additives. Contact of SE and CAM even during volume changes has to be maintained, that is, the protective surface layer needs to show some flexibility. Also, interactions of the CAM surface with binder and/or solvents during processing have to be considered.

5.4. Modeling

Usually, modeling studies do not offer suggestions for improvements on the CAM level. Instead, they rather focus on optimizing the SE (i.e., achieving high ionic conductivity). In our opinion, this lowers the degree of freedom, and we encourage to rethink the CAM with other particle shapes, sizes, elastic properties etc., and to widen the range of materials to SC or conversion-type CAMs. In addition, sophisticated mechanical models that can be coupled to electrochemical and thermal models on the microstructure level are required to gain more insight into pressure and temperature effects.

6. Conclusions

In summary, we have outlined the specific challenges and resulting requirements for the application of inorganic CAMs in SSBs. In particular, we focused on compiling recent strategies to tailor specific CAMs with respect to certain requirements related to (chemo-)mechanics and interfacial degradation occurring upon cycling. However, we finally like to emphasize that the design of CAMs for SSB applications cannot be conducted without taking the nature of the utilized SE into account. More precisely, different types of CAMs may require different types of SEs with certain matching properties (i.e., hard CAM together with soft SE and vice versa). Thus, we believe that in the case of SSBs, novel approaches are needed to improve the performance of the respective composite cathodes, which may include large-scale machine-aided screening approaches to identify best possible material combinations. This becomes even more important as cathodes for SSBs not only need to be optimized from a materials perspective (i.e., intrinsic material properties and surface chemistry) but their integration into a composite cathode may lead to new effects on a cell level. Modeling approaches should also tackle (chemo-)mechanical and fabrication processes for SSB cathodes in order to mitigate stress and limit pore space as much as possible. Finally, we provide scientists in the field with a comprehensive CAM development guideline targeting improved (inorganic) SSBs.

Acknowledgements

P.M. and F.S. contributed equally to this work. This work has been partly funded by the BMBF cluster of competence for solid state batteries (FestBatt, Bundesministerium für Bildung und Forschung) grant identifiers 03XP0177A/03XP0430A (thiophosphate platform), 03XP0433A (characterization platform), and 03XP0180/03XP0431 (coordination project). F.S. thanks the Fond der Chemischen Industrie (FCI) for

financial support through a Liebig fellowship. The authors thank Christian Grupe and Elisa Monte for graphical assistance.

Open access funding enabled and organized by Projekt DEAL.

Conflict of Interest

The authors declare no conflict of interest.

Keywords

chemo-mechanics, electrochemical energy storage, lithium-ion batteries, microstructures, NCM, particle sizes, thiophosphates

Received: April 26, 2022

Revised: July 3, 2022

Published online:

- [1] J. Janek, W. G. Zeier, *Nat Energy* **2016**, *1*, 16141.
- [2] J. Chen, J. Wu, X. Wang, A. Zhou, Z. Yang, *Energy Storage Mater.* **2021**, *35*, 70.
- [3] Y.-K. Sun, *ACS Energy Lett.* **2020**, *5*, 3221.
- [4] S. Nanda, A. Gupta, A. Manthiram, *Adv. Energy Mater.* **2021**, *11*, 2000804.
- [5] Q. Dai, J. C. Kelly, L. Gaines, M. Wang, *Batteries* **2019**, *5*, 48.
- [6] Y. Qian, P. Niehoff, M. Börner, M. Grütze, X. Mönnighoff, P. Behrends, S. Nowak, M. Winter, F. M. Schappacher, *J. Power Sources* **2016**, *329*, 31.
- [7] E. Trevisanello, R. Ruess, G. Conforto, F. H. Richter, J. Janek, *Adv. Energy Mater.* **2021**, *11*, 2003400.
- [8] N. P. W. Pieczonka, Z. Liu, P. Lu, K. L. Olson, J. Moote, B. R. Powell, J.-H. Kim, *J. Phys. Chem. C* **2013**, *117*, 15947.
- [9] W. Cho, S.-M. Kim, J. H. Song, T. Yim, S.-G. Woo, K.-W. Lee, J.-S. Kim, Y.-J. Kim, *J. Power Sources* **2015**, *282*, 45.
- [10] T. Li, X.-Z. Yuan, L. Zhang, D. Song, K. Shi, C. Bock, *Electrochem. Energy Rev.* **2020**, *3*, 43.
- [11] F. Walther, R. Koerver, T. Fuchs, S. Ohno, J. Sann, M. Rohnke, W. G. Zeier, J. Janek, *Chem. Mater.* **2019**, *31*, 3745.
- [12] R. Koerver, F. Walther, I. Aygün, J. Sann, C. Dietrich, W. G. Zeier, J. Janek, *J. Mater. Chem. A* **2017**, *5*, 22750.
- [13] R. Ruess, S. Schweidler, H. Hemmelmann, G. Conforto, A. Bielefeld, D. A. Weber, J. Sann, M. T. Elm, J. Janek, *J. Electrochem. Soc.* **2020**, *167*, 100532.
- [14] R. Koerver, W. Zhang, L. de Biasi, S. Schweidler, A. O. Kondrakov, S. Kolling, T. Brezesinski, P. Hartmann, W. G. Zeier, J. Janek, *Energy Environ. Sci.* **2018**, *11*, 2142.
- [15] R. C. Agrawal, G. P. Pandey, *J. Phys. D: Appl. Phys.* **2008**, *41*, 223001.
- [16] J. C. Bachman, S. Muy, A. Grimaud, H.-H. Chang, N. Pour, S. F. Lux, O. Paschos, F. Maglia, S. Lupart, P. Lamp, L. Giordano, Y. Shao-Horn, *Chem. Rev.* **2016**, *116*, 140.
- [17] T. Famprikis, P. Canepa, J. A. Dawson, M. S. Islam, C. Masquelier, *Nat. Mater.* **2019**, *18*, 1278.
- [18] Z. Gao, H. Sun, L. Fu, F. Ye, Y. Zhang, W. Luo, Y. Huang, *Adv. Mater.* **2018**, *30*, e1705702.
- [19] K. H. Park, Q. Bai, D. H. Kim, D. Y. Oh, Y. Zhu, Y. Mo, Y. S. Jung, *Adv. Energy Mater.* **2018**, *8*, 1800035.
- [20] L. Long, S. Wang, M. Xiao, Y. Meng, *J. Mater. Chem. A* **2016**, *4*, 10038.
- [21] K. J. Kim, M. Balaish, M. Wadaguchi, L. Kong, J. L. M. Rupp, *Adv. Energy Mater.* **2021**, *11*, 2002689.
- [22] X. Li, J. Liang, X. Yang, K. R. Adair, C. Wang, F. Zhao, X. Sun, *Energy Environ. Sci.* **2020**, *13*, 1429.
- [23] J. P. Beaupain, K. Waetzig, S.-K. Otto, A. Henss, J. Janek, M. Malaki, A. Pokle, J. Müller, B. Butz, K. Volz, M. Kuszczok, A. Michaelis, *ACS Appl. Mater. Interfaces* **2021**, *13*, 47488.
- [24] J. R. Nair, L. Imholt, G. Brunklaus, M. Winter, *Electrochem. Soc. Interface* **2019**, *28*, 55.
- [25] S. P. Culver, R. Koerver, W. G. Zeier, J. Janek, *Adv. Energy Mater.* **2019**, *9*, 1900626.
- [26] T. Koç, F. Marchini, G. Rouse, R. Dugas, J.-M. Tarascon, *ACS Appl. Energy Mater.* **2021**, *4*, 13575.
- [27] S. Sun, C.-Z. Zhao, H. Yuan, Y. Lu, J.-K. Hu, J.-Q. Huang, Q. Zhang, *Mater. Futures* **2021**, *1*, 012101.
- [28] S. Randau, D. A. Weber, O. Kötz, R. Koerver, P. Braun, A. Weber, E. Ivers-Tiffée, T. Adermann, J. Kulisch, W. G. Zeier, F. H. Richter, J. Janek, *Nat. Energy* **2020**, *5*, 259.
- [29] N. Kaiser, S. Spannenberger, M. Schmitt, M. Cronau, Y. Kato, B. Roling, *J. Power Sources* **2018**, *396*, 175.
- [30] T. Shi, Q. Tu, Y. Tian, Y. Xiao, L. J. Miara, O. Kononova, G. Ceder, *Adv. Energy Mater.* **2020**, *10*, 1902881.
- [31] P. Minnmann, L. Quillman, S. Burkhardt, F. H. Richter, J. Janek, *J. Electrochem. Soc.* **2021**, *168*, 040537.
- [32] J. Park, K. T. Kim, D. Y. Oh, D. Jin, D. Kim, Y. S. Jung, Y. M. Lee, *Adv. Energy Mater.* **2020**, *10*, 2001563.
- [33] W. Zhang, D. A. Weber, H. Weigand, T. Arlt, I. Manke, D. Schröder, R. Koerver, T. Leichtweiss, P. Hartmann, W. G. Zeier, J. Janek, *ACS Appl. Mater. Interfaces* **2017**, *9*, 17835.
- [34] J. Kim, M. Eom, S. Noh, D. Shin, *J. Power Sources* **2013**, *244*, 476.
- [35] Y. J. Nam, D. Y. Oh, S. H. Jung, Y. S. Jung, *J. Power Sources* **2018**, *375*, 93.
- [36] A. Bielefeld, D. A. Weber, J. Janek, *J. Phys. Chem. C* **2019**, *123*, 1626.
- [37] A. Bielefeld, D. A. Weber, J. Janek, *ACS Appl. Mater. Interfaces* **2020**, *12*, 12821.
- [38] G. Deysher, P. Ridley, S.-Y. Ham, J.-M. Doux, Y.-T. Chen, E. A. Wu, D. H. Tan, A. Cronk, J. Jang, Y. S. Meng, *Mater. Today Phys.* **2022**, *24*, 100679.
- [39] D. Hlushkou, A. E. Reising, N. Kaiser, S. Spannenberger, S. Schlabach, Y. Kato, B. Roling, U. Tallarek, *J. Power Sources* **2018**, *396*, 363.
- [40] A. Bielefeld, D. A. Weber, R. Rueß, V. Glavas, J. Janek, *J. Electrochem. Soc.* **2022**, *169*, 020539.
- [41] G. F. Dewald, S. Ohno, J. G. C. Hering, J. Janek, W. G. Zeier, *Batteries Supercaps* **2021**, *4*, 183.
- [42] T. Asano, S. Yubuchi, A. Sakuda, A. Hayashi, M. Tatsumisago, *J. Electrochem. Soc.* **2017**, *164*, A3960.
- [43] F. Strauss, T. Bartsch, L. de Biasi, A.-Y. Kim, J. Janek, P. Hartmann, T. Brezesinski, *ACS Energy Lett.* **2018**, *3*, 992.
- [44] C. Park, S. Lee, K. Kim, M. Kim, S. Choi, D. Shin, *J. Electrochem. Soc.* **2019**, *166*, A5318.
- [45] V. Laue, N. Wolff, F. Röder, U. Krewer, *Energy Technol.* **2020**, *8*, 1801049.
- [46] J. H. Teo, F. Strauss, Đ. Tripković, S. Schweidler, Y. Ma, M. Bianchini, J. Janek, T. Brezesinski, *Cell Rep. Phys. Sci.* **2021**, *2*, 100465.
- [47] M. Ghidui, J. Ruhl, S. P. Culver, W. G. Zeier, *J. Mater. Chem. A* **2019**, *7*, 17735.
- [48] S. Ohno, R. Koerver, G. Dewald, C. Rosenbach, P. Titscher, D. Steckermeier, A. Kwade, J. Janek, W. G. Zeier, *Chem. Mater.* **2019**, *31*, 2930.
- [49] S. Ohno, C. Rosenbach, G. F. Dewald, J. Janek, W. G. Zeier, *Adv. Funct. Mater.* **2021**, *31*, 2010620.
- [50] M. Falco, S. Ferrari, G. B. Appetecchi, C. Gerbaldi, *Mol. Syst. Des. Eng.* **2019**, *4*, 850.
- [51] A. Neumann, S. Randau, K. Becker-Steinberger, T. Danner, S. Hein, Z. Ning, J. Marrow, F. H. Richter, J. Janek, A. Latz, *ACS Appl. Mater. Interfaces* **2020**, *12*, 9277.

- [52] M. Finsterbusch, T. Danner, C.-L. Tsai, S. Uhlenbruck, A. Latz, O. Guillon, *ACS Appl. Mater. Interfaces* **2018**, *10*, 22329.
- [53] G. Bucci, T. Swamy, Y.-M. Chiang, W. C. Carter, *J. Mater. Chem. A* **2017**, *5*, 19422.
- [54] C. S. Giménez, L. Helmers, C. Schilde, A. Diener, A. Kwade, *Chem. Eng. Technol.* **2020**, *43*, 819.
- [55] S. Yamakawa, S. Ohta, T. Kobayashi, *Solid State Ionics* **2020**, *344*, 115079.
- [56] A. Ohashi, M. Kodama, S. Xueying, S. Hori, K. Suzuki, R. Kanno, S. Hirai, *J. Power Sources* **2020**, *470*, 228437.
- [57] M. B. Dixit, A. Parejiya, N. Muralidharan, R. Essehli, R. Amin, I. Belharouak, *Energy Storage Mater.* **2021**, *40*, 239.
- [58] S. Randau, F. Walther, A. Neumann, Y. Schneider, R. S. Negi, B. Mogwitz, J. Sann, K. Becker-Steinberger, T. Danner, S. Hein, A. Latz, F. H. Richter, J. Janek, *Chem. Mater.* **2021**, *33*, 1380.
- [59] D. Bistri, A. Afshar, C. V. Di Leo, *Meccanica* **2021**, *56*, 1523.
- [60] J.-M. Doux, Y. Yang, D. H. S. Tan, H. Nguyen, E. A. Wu, X. Wang, A. Banerjee, Y. S. Meng, *J. Mater. Chem. A* **2020**, *8*, 5049.
- [61] D. H. S. Tan, E. A. Wu, H. Nguyen, Z. Chen, M. A. T. Marple, J.-M. Doux, X. Wang, H. Yang, A. Banerjee, Y. S. Meng, *ACS Energy Lett.* **2019**, *4*, 2418.
- [62] R. Usiskin, J. Maier, *J. Electrochem. Soc.* **2020**, *167*, 080505.
- [63] D. Y. Oh, Y. J. Nam, K. H. Park, S. H. Jung, K. T. Kim, A. R. Ha, Y. S. Jung, *Adv. Energy Mater.* **2019**, *9*, 1802927.
- [64] S. Ito, S. Fujiki, T. Yamada, Y. Aihara, Y. Park, T. Y. Kim, S.-W. Baek, J.-M. Lee, S. Doo, N. Machida, *J. Power Sources* **2014**, *248*, 943.
- [65] T. Inada, *Solid State Ionics* **2003**, *158*, 275.
- [66] F. Hippauf, B. Schumm, S. Doerfler, H. Althues, S. Fujiki, T. Shiratsuchi, T. Tsujimura, Y. Aihara, S. Kaskel, *Energy Storage Mater.* **2019**, *21*, 390.
- [67] M. Yamamoto, Y. Terauchi, A. Sakuda, M. Takahashi, *Sci. Rep.* **2018**, *8*, 1212.
- [68] Y. Xiao, K. Turcheniuk, A. Narla, A.-Y. Song, X. Ren, A. Magasinski, A. Jain, S. Huang, H. Lee, G. Yushin, *Nat. Mater.* **2021**, *20*, 984.
- [69] R. E. Usiskin, J. Maier, *Phys. Chem. Chem. Phys.* **2018**, *20*, 16449.
- [70] A. van der Ven, J. Bhattacharya, A. A. Belak, *Acc. Chem. Res.* **2013**, *46*, 1216.
- [71] Y. Zhu, C. Wang, *J. Phys. Chem. C* **2010**, *114*, 2830.
- [72] L. Froboese, J. F. van der Sichel, T. Loellhoffel, L. Helmers, A. Kwade, *J. Electrochem. Soc.* **2019**, *166*, A318.
- [73] S. Brutti, G. Greco, P. Reale, S. Panero, *Electrochim. Acta* **2013**, *106*, 483.
- [74] D. Wang, X. Wu, Z. Wang, L. Chen, *J. Power Sources* **2005**, *140*, 125.
- [75] Q. Liu, Y. Liu, F. Yang, H. He, X. Xiao, Y. Ren, W. Lu, E. Stach, J. Xie, *ACS Appl. Mater. Interfaces* **2018**, *10*, 4622.
- [76] L. de Biasi, A. O. Kondrakov, H. Geßwein, T. Brezesinski, P. Hartmann, J. Janek, *J. Phys. Chem. C* **2017**, *121*, 26163.
- [77] S. Payandeh, D. Goonetilleke, M. Bianchini, J. Janek, T. Brezesinski, *Curr. Opin. Electrochem.* **2022**, *31*, 100877.
- [78] H. Jeon, D.-H. Kwon, H. Kim, J.-H. Lee, Y. Jun, J.-W. Son, S. Park, *Chem. Eng. J.* **2022**, *445*, 136828.
- [79] F. Strauss, L. de Biasi, A.-Y. Kim, J. Hertle, S. Schweidler, J. Janek, P. Hartmann, T. Brezesinski, *ACS Mater. Lett.* **2020**, *2*, 84.
- [80] A. Banerjee, X. Wang, C. Fang, E. A. Wu, Y. S. Meng, *Chem. Rev.* **2020**, *120*, 6878.
- [81] S. H. Jung, U.-H. Kim, J.-H. Kim, S. Jun, C. S. Yoon, Y. S. Jung, Y.-K. Sun, *Adv. Energy Mater.* **2020**, *10*, 1903360.
- [82] F. Strauss, J. H. Teo, J. Maibach, A.-Y. Kim, A. Mazilkin, J. Janek, T. Brezesinski, *ACS Appl. Mater. Interfaces* **2020**, *12*, 57146.
- [83] W. Zhang, F. H. Richter, S. P. Culver, T. Leichtweiss, J. G. Lozano, C. Dietrich, P. G. Bruce, W. G. Zeier, J. Janek, *ACS Appl. Mater. Interfaces* **2018**, *10*, 22226.
- [84] A.-Y. Kim, F. Strauss, T. Bartsch, J. H. Teo, J. Janek, T. Brezesinski, *Sci. Rep.* **2021**, *11*, 5367.
- [85] F. Walther, F. Strauss, X. Wu, B. Mogwitz, J. Hertle, J. Sann, M. Rohnke, T. Brezesinski, J. Janek, *Chem. Mater.* **2021**, *33*, 2110.
- [86] Y. Han, S. H. Jung, H. Kwak, S. Jun, H. H. Kwak, J. H. Lee, S.-T. Hong, Y. S. Jung, *Adv. Energy Mater.* **2021**, *11*, 2100126.
- [87] S. Sen, E. Trevisanello, E. Niemöller, B.-X. Shi, F. J. Simon, F. H. Richter, *J. Mater. Chem. A* **2021**, *9*, 18701.
- [88] M. Weiss, R. Ruess, J. Kasnatscheew, Y. Levartovsky, N. R. Levy, P. Minnmann, L. Stolz, T. Waldmann, M. Wohlfahrt-Mehrens, D. Aurbach, M. Winter, Y. Ein-Eli, J. Janek, *Adv. Energy Mater.* **2021**, *11*, 2101126.
- [89] A. J. Merryweather, C. Schnedermann, Q. Jacquet, C. P. Grey, A. Rao, *Nature* **2021**, *594*, 522.
- [90] S. Wang, R. Fang, Y. Li, Y. Liu, C. Xin, F. H. Richter, C.-W. Nan, *J. Materiomics* **2021**, *7*, 209.
- [91] G. Conforto, R. Ruess, D. Schröder, E. Trevisanello, R. Fantin, F. H. Richter, J. Janek, *J. Electrochem. Soc.* **2021**, *168*, 070546.
- [92] K. Takada, N. Ohta, L. Zhang, K. Fukuda, I. Sakaguchi, R. Ma, M. Osada, T. Sasaki, *Solid State Ionics* **2008**, *179*, 1333.
- [93] Y.-Q. Zhang, Y. Tian, Y. Xiao, L. J. Miara, Y. Aihara, T. Tsujimura, T. Shi, M. C. Scott, G. Ceder, *Adv. Energy Mater.* **2020**, *10*, 1903778.
- [94] R. S. Negi, P. Minnmann, R. Pan, S. Ahmed, M. J. Herzog, K. Volz, R. Takata, F. Schmidt, J. Janek, M. T. Elm, *Chem. Mater.* **2021**, *33*, 6713.
- [95] Y. Zhao, K. Zheng, X. Sun, *Joule* **2018**, *2*, 2583.
- [96] A. Gurung, J. Pokharel, A. Baniya, R. Pathak, K. Chen, B. S. Lamsal, N. Ghimire, W.-H. Zhang, Y. Zhou, Q. Qiao, *Sustainable Energy Fuels* **2019**, *3*, 3279.
- [97] M. Yoon, Y. Dong, J. Hwang, J. Sung, H. Cha, K. Ahn, Y. Huang, S. J. Kang, J. Li, J. Cho, *Nat. Energy* **2021**, *6*, 362.
- [98] A.-Y. Kim, F. Strauss, T. Bartsch, J. H. Teo, T. Hatsukade, A. Mazilkin, J. Janek, P. Hartmann, T. Brezesinski, *Chem. Mater.* **2019**, *31*, 9664.
- [99] S. Deng, Q. Sun, M. Li, K. Adair, C. Yu, J. Li, W. Li, J. Fu, X. Li, R. Li, Y. Hu, N. Chen, H. Huang, L. Zhang, S. Zhao, S. Lu, X. Sun, *Energy Storage Mater.* **2021**, *35*, 661.
- [100] T. A. Yersak, H. A. Macpherson, S. C. Kim, V.-D. Le, C. S. Kang, S.-B. Son, Y.-H. Kim, J. E. Trevey, K. H. Oh, C. Stoldt, S.-H. Lee, *Adv. Energy Mater.* **2013**, *3*, 120.
- [101] Y. Zhang, X. Sun, D. Cao, G. Gao, Z. Yang, H. Zhu, Y. Wang, *Energy Storage Mater.* **2021**, *41*, 505.
- [102] F. Strauss, S. Payandeh, A. Kondrakov, T. Brezesinski, *Mater. Futures* **2022**, *1*, 023501.
- [103] D. Kitsche, Y. Tang, Y. Ma, D. Goonetilleke, J. Sann, F. Walther, M. Bianchini, J. Janek, T. Brezesinski, *ACS Appl. Energy Mater.* **2021**, *4*, 7338.
- [104] R. Fantin, E. Trevisanello, R. Ruess, A. Pokle, G. Conforto, F. H. Richter, K. Volz, J. Janek, *Chem. Mater.* **2021**, *33*, 2624.
- [105] S. Payandeh, F. Strauss, A. Mazilkin, A. Kondrakov, T. Brezesinski, *Nano Res. Energy* **2022**, *1*, <https://doi.org/10.26599/NRE.2022.9120016>.
- [106] Y. Ma, J. H. Teo, F. Walther, Y. Ma, R. Zhang, A. Mazilkin, Y. Tang, D. Goonetilleke, J. Janek, M. Bianchini, T. Brezesinski, *Adv. Funct. Mater.* **2022**, *32*, 2111829.
- [107] S. Neudeck, F. Strauss, G. Garcia, H. Wolf, J. Janek, P. Hartmann, T. Brezesinski, *Chem. Commun.* **2019**, *55*, 2174.
- [108] R. S. Negi, S. P. Culver, A. Mazilkin, T. Brezesinski, M. T. Elm, *ACS Appl. Mater. Interfaces* **2020**, *12*, 31392.
- [109] J. H. Teo, F. Strauss, F. Walther, Y. Ma, S. Payandeh, T. Scherer, M. Bianchini, J. Janek, T. Brezesinski, *Mater. Futures* **2022**, *1*, 015102.
- [110] F. Strauss, J. H. Teo, A. Schiele, T. Bartsch, T. Hatsukade, P. Hartmann, J. Janek, T. Brezesinski, *ACS Appl. Mater. Interfaces* **2020**, *12*, 20462.
- [111] A. Liu, N. Zhang, H. Li, J. Inglis, Y. Wang, S. Yin, H. Wu, J. R. Dahn, *J. Electrochem. Soc.* **2019**, *166*, A4025.

- [112] A. Aishova, G.-T. Park, C. S. Yoon, Y.-K. Sun, *Adv. Energy Mater.* **2020**, *10*, 1903179.
- [113] Z.-Y. Li, H. Guo, X. Ma, K. Sun, D. Chen, L. He, S. Han, *J. Phys. Chem. C* **2019**, *123*, 19298.
- [114] H. Li, A. Liu, N. Zhang, Y. Wang, S. Yin, H. Wu, J. R. Dahn, *Chem. Mater.* **2019**, *31*, 7574.
- [115] J. Langdon, A. Manthiram, *Energy Storage Mater.* **2021**, *37*, 143.
- [116] A. Liu, N. Zhang, J. E. Stark, P. Arab, H. Li, J. R. Dahn, *J. Electrochem. Soc.* **2021**, *168*, 050506.
- [117] C. Doerrer, I. Capone, S. Narayanan, J. Liu, C. R. M. Grovenor, M. Pasta, P. S. Grant, *ACS Appl. Mater. Interfaces* **2021**, *13*, 37809.
- [118] J. Zhu, G. Chen, *J. Mater. Chem. A* **2019**, *7*, 5463.
- [119] J. Zhu, S. Sharifi-Asl, J. C. Garcia, H. H. Iddir, J. R. Croy, R. Shahbazian-Yassar, G. Chen, *ACS Appl. Energy Mater.* **2020**, *3*, 4799.
- [120] X. Liu, B. Zheng, J. Zhao, W. Zhao, Z. Liang, Y. Su, C. Xie, K. Zhou, Y. Xiang, J. Zhu, H. Wang, G. Zhong, Z. Gong, J. Huang, Y. Yang, *Adv. Energy Mater.* **2021**, *11*, 2003583.
- [121] L. Zheng, J. C. Bennett, M. N. Obrovac, *J. Electrochem. Soc.* **2020**, *167*, 130536.
- [122] F. Strauss, D. Stepien, J. Maibach, L. Pfaffmann, S. Indris, P. Hartmann, T. Brezesinski, *RSC Adv.* **2020**, *10*, 1114.
- [123] F. Walther, S. Randau, Y. Schneider, J. Sann, M. Rohnke, F. H. Richter, W. G. Zeier, J. Janek, *Chem. Mater.* **2020**, *32*, 6123.
- [124] W. Zhang, T. Leichtweiß, S. P. Culver, R. Koerver, D. Das, D. A. Weber, W. G. Zeier, J. Janek, *ACS Appl. Mater. Interfaces* **2017**, *9*, 35888.
- [125] C. Wang, J. Hong, *Electrochem. Solid-State Lett.* **2007**, *10*, A65.
- [126] J. Auvergniot, A. Cassel, J.-B. Ledeuil, V. Viallet, V. Seznec, R. Dedryvère, *Chem. Mater.* **2017**, *29*, 3883.
- [127] H. Kitaura, A. Hayashi, K. Tadanaga, M. Tatsumisago, *J. Electrochem. Soc.* **2010**, *157*, A407.
- [128] G. Oh, M. Hirayama, O. Kwon, K. Suzuki, R. Kanno, *Chem. Mater.* **2016**, *28*, 2634.
- [129] S. Yubuchi, Y. Ito, T. Matsuyama, A. Hayashi, M. Tatsumisago, *Solid State Ionics* **2016**, *285*, 79.
- [130] G. Liu, Y. Lu, H. Wan, W. Weng, L. Cai, Z. Li, X. Que, H. Liu, X. Yao, *ACS Appl. Mater. Interfaces* **2020**, *12*, 28083.
- [131] L. Zhang, D. Sun, J. Kang, J. Feng, H. A. Bechtel, L.-W. Wang, E. J. Cairns, J. Guo, *Nano Lett.* **2018**, *18*, 1466.
- [132] A. Débart, L. Dupont, R. Patrice, J.-M. Tarascon, *Solid State Sci.* **2006**, *8*, 640.
- [133] B. Jache, B. Mogwitz, F. Klein, P. Adelhelm, *J. Power Sources* **2014**, *247*, 703.
- [134] S.-H. Yu, X. Feng, N. Zhang, J. Seok, H. D. Abruña, *Acc. Chem. Res.* **2018**, *51*, 273.
- [135] S. S. Zhang, D. T. Tran, *Electrochim. Acta* **2015**, *176*, 784.
- [136] X. Hua, A. S. Eggeman, E. Castillo-Martínez, R. Robert, H. S. Geddes, Z. Lu, C. J. Pickard, W. Meng, K. M. Wiaderek, N. Pereira, G. G. Amatucci, P. A. Midgley, K. W. Chapman, U. Steiner, A. L. Goodwin, C. P. Grey, *Nat. Mater.* **2021**, *20*, 841.
- [137] S.-H. Chung, A. Manthiram, *Adv. Mater.* **2019**, *31*, e1901125.
- [138] Q. Pang, X. Liang, C. Y. Kwok, L. F. Nazar, *Nat. Energy* **2016**, *1*, 16132.
- [139] S. Dörfler, H. Althues, P. Härtel, T. Abendroth, B. Schumm, S. Kaskel, *Joule* **2020**, *4*, 539.
- [140] L. Medenbach, P. Adelhelm, in *Electrochemical Energy Storage* (Ed: R.-A. Eichel), Springer International Publishing, Cham **2019**, p. 101.
- [141] L. Li, M. Cabán-Acevedo, S. N. Girard, S. Jin, *Nanoscale* **2014**, *6*, 2112.
- [142] E. Strauss, *J. Power Sources* **2003**, *115*, 323.
- [143] K. Takada, *Solid State Ionics* **1999**, *117*, 273.
- [144] G. F. Dewald, Z. Liaqat, M. A. Lange, W. Tremel, W. G. Zeier, *Angew. Chem.* **2021**, *133*, 18096.
- [145] K. Okamoto, S. Kawai, *Jpn. J. Appl. Phys.* **1973**, *12*, 1130.
- [146] A. L. Santhosha, N. Nazer, R. Koerver, S. Randau, F. H. Richter, D. A. Weber, J. Kulisch, T. Adermann, J. Janek, P. Adelhelm, *Adv. Energy Mater.* **2020**, *10*, 2002394.
- [147] H. Wang, X. Cao, W. Liu, X. Sun, *Front. Energy Res.* **2019**, *7*, 112.
- [148] B. Ding, J. Wang, Z. Fan, S. Chen, Q. Lin, X. Lu, H. Dou, A. K. Nanjundan, G. Yushin, X. Zhang, Y. Yamauchi, *Mater. Today* **2020**, *40*, 114.
- [149] N. H. H. Phuc, K. Hikima, H. Muto, A. Matsuda, *Crit. Rev. Solid State Mater. Sci.* **2021**, *47*, 283.
- [150] S. Ohno, W. G. Zeier, *Acc. Mater. Res.* **2021**, *2*, 869.
- [151] A. Hayashi, T. Ohtomo, F. Mizuno, K. Tadanaga, M. Tatsumisago, *Electrochem. Commun.* **2003**, *5*, 701.
- [152] U. Ulissi, S. Ito, S. M. Hosseini, A. Varzi, Y. Aihara, S. Passerini, *Adv. Energy Mater.* **2018**, *8*, 1801462.
- [153] A. Douglas, R. Carter, L. Oakes, K. Share, A. P. Cohn, C. L. Pint, *ACS Nano* **2015**, *9*, 11156.
- [154] S. M. Hosseini, A. Varzi, S. Ito, Y. Aihara, S. Passerini, *Energy Storage Mater.* **2020**, *27*, 61.
- [155] S. Wang, M. Tang, Q. Zhang, B. Li, S. Ohno, F. Walther, R. Pan, X. Xu, C. Xin, W. Zhang, L. Li, Y. Shen, F. H. Richter, J. Janek, C.-W. Nan, *Adv. Energy Mater.* **2021**, *11*, 2101370.
- [156] W. Ji, X. Zhang, D. Zheng, H. Huang, T. H. Lambert, D. Qu, *Adv. Funct. Mater.* **2022**, *23*, 2202919.
- [157] Z. Yang, F. Wang, Z. Hu, J. Chu, H. Zhan, X. Ai, Z. Song, *Adv. Energy Mater.* **2021**, *11*, 2102962.
- [158] J. Zhang, Z. Chen, Q. Ai, T. Terlier, F. Hao, Y. Liang, H. Guo, J. Lou, Y. Yao, *Joule* **2021**, *5*, 1845.



Philip Minnmann obtained his B.Sc. and M.Sc. in material science from the RWTH Aachen University and subsequently joined the research group of Prof. Jürgen Janek at Justus-Liebig University Gießen as a Ph.D. student. His main research focus is on the experimental investigation of composite cathodes for solid-state batteries and the influence of microstructural features on cathode kinetics.



Florian Strauss obtained his Ph.D. in France and Slovenia (2016) under the supervision of Prof. Tarascon (Collège de France, Paris) and Prof. Dominko (National Institute of Chemistry, Ljubljana). He was then a postdoctoral fellow at BELLA (KIT), investigating different aspects of solid-state Li-ion batteries, and now directs his own research on the exploration of novel solid electrolytes supported by a Liebig fellowship at BELLA.



Anja Bielefeld is a junior group leader for modeling electrochemical systems at the Center for Materials Research of the Justus-Liebig University Gießen. She recently obtained her Ph.D. degree from the Justus-Liebig University on models for solid-state battery composite cathodes in cooperation with Volkswagen AG. She is particularly interested in microstructure effects and their influence on the cell properties.



Torsten Brezesinski is a chemist by training, earning his doctorate in physical chemistry from the MPI of Colloids and Interfaces/University of Potsdam in 2005. He is laboratory manager of the KIT/BASF SE joint laboratory for batteries and electrochemistry (BELLA) and Group Leader at the Institute of Nanotechnology at KIT. His work encompasses the characterization of next-generation battery materials for electrochemical energy storage and the design of mesoporous metal oxides.



Felix H. Richter is a junior research group leader in physical chemistry, materials science, and characterization at the Center for Materials Research of the Justus-Liebig-University Gießen. He is particularly interested in concepts that bridge the properties of inorganic materials and polymers. Currently, the Richter workgroup specializes in analyzing the fundamental transport mechanisms of ions across the interfaces of different battery components and the development of hybrid approaches for solid-state batteries. In March 2020, he received the NanoMatFutur funding by the Federal Ministry for Education and Research on the topic of solid-state batteries with lithium metal and polymer protective coatings.



Jürgen Janek holds a chair for physical chemistry at Justus-Liebig-University in Gießen (Germany) and is scientific director of BELLA, a joint lab of BASF SE and KIT in Karlsruhe/Germany. He received his doctoral degree in physical chemistry and was visiting professor at Seoul National University, Tohoku University, and Université d'Aix-Marseille. His research spans a wide range from transport studies in mixed conductors and at interfaces to in situ studies in electrochemical cells. Current key interests include all-solid state batteries, solid electrolytes, and solid electrolyte interfaces. He is particularly interested in kinetics at interfaces.